# Titanium Nitride Thin Films by the Electron Shower Process

by

Patrick R. LeClair

Submitted to the Department of Materials Science and Engineering in partial fulfillment of the requirements for the degree of

Bachelor of Science in Materials Science and Engineering

at the

MASSACHUSETTS INSTITUTE OF TECHNOLOGY

May 1998

© Massachusetts Institute of Technology 1998. All rights reserved.

Author ..........................................................
Department of Materials Science and Engineering
May 8, 1998

Certified by ..........................................................
Jagadeesh S. Moodera
Research Scientist, Francis Bitter Magnet Laboratory
Thesis Supervisor

Certified by ..........................................................
Caroline A. Ross
Assistant Professor of Materials Science and Engineering
Thesis Supervisor

Accepted by ..........................................................
David Roylance
Executive Officer, Department of Materials Science and Engineering

ARCHIVES

JUN 24 1998

# Titanium Nitride Thin Films by the Electron Shower Process

by

Patrick R. LeClair

Submitted to the Department of Materials Science and Engineering
on May 8, 1998, in partial fulfillment of the
requirements for the degree of
Bachelor of Science in Materials Science and Engineering

## Abstract

Titanium nitride (TiN), a stable compound with the NaCl structure, has a wide range of properties which find applications in cutting tools, wear resistant parts, semiconductor metallization, and the jewelry industry. However, there are problems with preparing highly adhesive thin films which maintain good properties. Thin films of titanium nitride have been prepared by the Electron Shower (ES) and Enhanced Activated Reactive Evaporation (EARE) processes. These films exhibit extremely high adhesion to glass and other substrates, and good optical and electronic properties. Several analytical techniques such as X-ray diffraction (XRD), resistivity *vs.* temperature, Atomic Force Microscopy (AFM), and UV-Visible-NIR spectroscopy, were utilized to characterize the films. AFM images indicate a fine-grained columnar microstructure, with 20-150nm grain size. Resistivities $\sim 200\mu\Omega\cdot$cm at room temperature were obtained, generally decreasing as temperature decreases. Infrared reflection of up to 70% was obtained, with good wavelength selectivity. These properties are nearly as good as the best values reported in the literature. Finally, it is shown that the ES/EARE processes can produce high quality TiN films with good adhesion.

Thesis Supervisor: Jagadeesh S. Moodera
Title: Research Scientist, Francis Bitter Magnet Laboratory

Thesis Supervisor: Caroline A. Ross
Title: Associate Professor of Materials Science and Engineering

# Acknowledgments

I would like to thank Dr. Jagadeesh Moodera for his invaluable suggestions and unwavering support. Everything I know about research has come from him. I would also like to thank Prof. C.A. Ross for agreeing to serve as my faculty advisor, and providing advice when I needed it.

A special acknowledgement goes to Dr. Janusz Nowak, who has always put aside his own projects to help me when I need assistance. His vast experience and creativity helped me greatly along the way, and were essential to the completion of this thesis. Further, Dr. Nowak is one of the most enjoyable people I have ever worked with. Also thanks to C. Tanaka, R. Jansen, and R. van der Veerdonk for providing helpful advice, and to N. Friedman for his patience in listening to my troubles.

And last, but not least, thanks to my parents Roy and Fay LeClair who encouraged me all along and helped my through the difficult times.

# Contents

Acknowledgements 3

1 Introduction and Motivation 9

1.1 Introduction . . . . . . . . . . . . . . . . . . . . . . . . . . . 9

1.2 Motivation . . . . . . . . . . . . . . . . . . . . . . . . . . . 9

2 Titanium Nitride 12

2.1 General Properties . . . . . . . . . . . . . . . . . . . . . . . 12

3 Preparation 19

3.1 Enhanced Activated Reactive Evaporation . . . . . . . . . . . . . . . 19

3.2 Electron Shower . . . . . . . . . . . . . . . . . . . . . . . . . 20

3.3 ES/EARE Apparatus and Procedure . . . . . . . . . . . . . . . . . . 21

3.3.1 Modifications . . . . . . . . . . . . . . . . . . . . . . . 24

4 Characterization and Results 26

4.1 X-ray Diffraction . . . . . . . . . . . . . . . . . . . . . . . . 26

4.1.1 Lattice Parameter . . . . . . . . . . . . . . . . . . . . . 26

4.1.2 Crystallinity, Other Phases Present . . . . . . . . . . . . . . . 29

4.1.3 Peak Heights . . . . . . . . . . . . . . . . . . . . . . . . 30

4.2 Atomic Force Microscopy . . . . . . . . . . . . . . . . . . . . . 32

4.2.1 Roughness and Grain Size . . . . . . . . . . . . . . . . . . 32

4.2.2 Grain Structure . . . . . . . . . . . . . . . . . . . . . . . 33

4.3 UV-Visible-NIR Spectroscopy . . . . . . . . . . . . . . . . . . . 36

4.4 Resistivity vs. Temperature . . . . . . . . . . . . . . . . . . . . . . . . 36
4.5 Post Deposition Annealing . . . . . . . . . . . . . . . . . . . . . . . . 38
4.5.1 Effect on Resistivity . . . . . . . . . . . . . . . . . . . . . . . 40
4.5.2 Effect on Microstructure . . . . . . . . . . . . . . . . . . . . . 41
4.6 Adhesion . . . . . . . . . . . . . . . . . . . . . . . . . . . . . . . . 42

**5 Discussion** **44**
5.1 Apparatus Characteristics . . . . . . . . . . . . . . . . . . . . . . . . 44
5.2 X-ray Diffraction . . . . . . . . . . . . . . . . . . . . . . . . . . . . 45
5.3 UV-Visible-NIR . . . . . . . . . . . . . . . . . . . . . . . . . . . . . 46
5.4 Atomic Force Microscopy . . . . . . . . . . . . . . . . . . . . . . . . 48
5.5 Resistivity *vs.* Temperature . . . . . . . . . . . . . . . . . . . . . . 48

**6 Conclusions, Recommendations** **51**
6.1 Conclusion . . . . . . . . . . . . . . . . . . . . . . . . . . . . . . . 51
6.2 Future Recommendations . . . . . . . . . . . . . . . . . . . . . . . . 51

**A Reactive Deposition and Plasma Chemistry** **56**
A.1 General Aspects of Reactive Deposition . . . . . . . . . . . . . . . . . 56
A.2 Reactions and Species Present . . . . . . . . . . . . . . . . . . . . . . 58
A.2.1 Plasma Discharge Volume . . . . . . . . . . . . . . . . . . . . 58
A.2.2 Plasma-Surface Interactions . . . . . . . . . . . . . . . . . . . 62

**B X-ray Diffraction Data** **64**

**C Resistivity *vs.* Temperature Data** **65**

# List of Figures


2-1 Ti-N Phase Diagram . . . . . . . . . . . . . . . . . . . . . . . . . . 15

2-2 $\delta$-TiN (Fm$\bar{3}$m, a=4.24Å) Band Structure . . . . . . . . . . . . . . . . . 16

2-3 Lattice Parameter vs. Composition for $TiN_x$ . . . . . . . . . . . . . . 18

3-1 Electron Shower/EARE Apparatus. . . . . . . . . . . . . . . . . . . . . . 22

4-1 X-ray Diffraction Pattern for 9-207. . . . . . . . . . . . . . . . . . . . . 27

4-2 X-ray Diffraction Pattern for 9-210. . . . . . . . . . . . . . . . . . . . . 27

4-3 X-ray Diffraction Pattern for 9-210. . . . . . . . . . . . . . . . . . . . . 28

4-4 X-ray Diffraction Pattern for 9-213. . . . . . . . . . . . . . . . . . . . . 28

4-5 XRD (111)/(200) Peak Intensity Ratios for Prepared Samples. . . . . 31

4-6 AFM Images. . . . . . . . . . . . . . . . . . . . . . . . . . . . . . 34

4-7 Roughness (A) and Grain Size (B) *vs.* substrate temperature. . . . . 35

4-8 Reflection and Transmission *vs.* Wavelength. . . . . . . . . . . . . . . 37

4-9 Resistivity *vs.* Temperature for 9-212 and 9-216 . . . . . . . . . . . . 39

4-10 Effect of $N_2$ or vacuum annealing on resitivity *vs.* temperature behavior. 41

5-1 (200) to (111) Peak Ratio *vs.* Substrate Temperature. . . . . . . . . . 47

A-1 Schematic of $N_2$ Plasma Reactions. . . . . . . . . . . . . . . . . . . . 61

# List of Tables


2.1 Properties of Ti and TiN, at Room Temperature . . . . . . . . . . . . . 14

2.2 Phases of Ti and $TiN_x$ . . . . . . . . . . . . . . . . . . . . . . . . . 15

2.3 Enthalpies and Entropies of Formation at 298K for Selected Compounds 18

3.1 Process Parameters . . . . . . . . . . . . . . . . . . . . . . . . . . . 23

4.1 Calculated Lattice Parameters . . . . . . . . . . . . . . . . . . . . . . 29

4.2 Resistivity of TiN samples on glass. . . . . . . . . . . . . . . . . . . . 39

4.3 Resistivity of reported TiN samples. . . . . . . . . . . . . . . . . . . . 40

4.4 Effect of Vacuum or $N_2$ Annealing on Microstructure, 9-213G . . . . 42

A.1 Plasma Volume and Surface Reactions: $N_2$, Ti, and $e^-$. . . . . . . . . 59

# List of Symbols

**Å** – Angstrom unit, $10^{-10}$m.

**a,c** – Lattice constant; a alone refers to cubic systems.

$\alpha$, $\beta$ – hcp and bcc phases of Ti, respectively.

$\epsilon$ – One of the two phases of $Ti_2N$, 33% at. N.

$\delta'$ – One of the two phases of $Ti_2N$; ~38 at. % N.

$\delta$ – Major nitride phase TiN.

**ITO** – Indium Tin Oxide, $InSnO_x$.

**ARE** – Activated Reactive Evaporation.

**EARE** – Enhanced Activated Reactive Evaporation.

**ES** – Electron Shower.

$\mathbf{V}_a$ – Voltage (dc) applied to accelerating anode.

$\mathbf{V}_b$ – Voltage (dc) applied to substrate.

$\mathbf{I}_{sg}$ – Current (dc) between substrate and ground.

$\mathbf{R}_{std}$ – Precision standard resistor for measurement of $I_{sg}$.

$\mathbf{T}_s$ – Substrate temperature, °C.

$\mathbf{T}_c$ – Superconductive transition temperature, K.

$\mathbf{t}_{ti}$ – Ti thickness.

$\dot{t}_{Ti}$ – Ti deposition rate.

$\mathbf{P}_{N_2}$ – $N_2$ pressure in chamber.

$\lambda_{mfp}$ – Mean free path, cm.

$\mathbf{I}_{200}$ – Background corrected intensity of (200) X-ray diffraction peak.

$\mathbf{I}_{111}$ – Background corrected intensity of (111) X-ray diffraction peak.

**TEM** – Transmission Electron Microscopy.

**STM** – Scanning Tunneling Microscopy.

**AFM** – Atomic Force Microscopy.

**XRF** – X-ray Fluorescence.

**XPS** – X-ray Photoelectron Spectroscopy.

# Chapter 1

# Introduction and Motivation

## 1.1 Introduction

Titanium Nitride is a material which has many remarkable properties (see table 2.1), properties which lend themselves to a wide range of applications. Correspondingly, titanium nitride coatings have successfully been used in a number of applications. Its high hardness and corrosion resistance has made it particularly useful for increasing the wear resistance of high speed steel cutting tools [1], while its high conductivity and diffusion barrier properties have led to its employment in semiconductor metallization schemes [2]. In addition, TiN films have been used for cosmetic faux gold surfaces [3] (such as watch bezels, watch bands, and pen barrels [4]), wavelength-selective transparent optical films [5], thin film resistors, tool bit coatings, and, due to its strong infrared reflection, energy-saving coatings for windows.

## 1.2 Motivation

Despite the great appeal of titanium nitride coatings, there are several problems with existing coating methods which limit the use of such coatings. For example, conventional Chemical Vapor Deposition (CVD) methods for depositing nitride thin films require high temperatures [6] ($\sim$800°C is common), which can be quite undesirable

(*e.g.*, in the case of coating steel tool bits). CVD coating also utilizes toxic precurser gases (*e.g.*, $TiCl_4$), and has toxic exhaust gases (*e.g.*, HCl, Cl). Many compounds cannot be directly deposited (non reactively) due to decomposition or dissociation. In many cases reactive deposition of some sort is the only practical, or possible, option. Reactive sputtering has been successfully used for the deposition of TiN, but often deposition rates are low. Other deposition methods, such as reactive evaporation, can produce films with poor adhesion to the substrate, poor optical properties, poor mechanical properties, *etc*, or combinations thereof [7].

In addition to problems of methodology, more basic limitations exist in the case of nitride coatings (as well as for other compounds). For many technologically important nitrides (*e.g.*, TiN, ZrN, $Si_3N_4$), the free energy of compound formation can be relatively low, especially when compared to the oxides (*e.g.*, $TiO_2$, $ZrO_2$). Thus, reactive sputtering and conventional reactive evaporation may still not be viable options, even if the problems of methodology are essentially solved. Energetic and kinetic factors governing compound formation during deposition may lead to a low reaction yield. Given the problems with many of the existing coating techniques, the further development of attractive alternative methods is extremely important.

In this work, we have investigated two hybrid Physical Vapor Deposition (PVD) techniques for fabricating high quality titanium nitride films, with a view to the more general case of reactive compound deposition. The processes investigated, the "electron shower" process [7], and Enhanced Activated Reactive Evaporation [8], solve many of the problems of other coating techniques, and can be attractive alternatives to CVD and other methods. However, these processes are underdeveloped and not completely understood. This work focuses on fabricating titanium nitride films by both of these novel methods in order to assess the advantages they may have over conventional deposition methods.

External properties of the prepared films have been characterized and examined

in relation to process variables, elucidating the relation of material properties to processing. The focus of this investigation is twofold: first, to find a reasonable set of conditions for producing high quality titanium nitride films; and second, to illuminate more general aspects of the processes used. Chapter 2 gives an overview of titanium nitride and its properties. Chapter 3 outlines the processes used in this work. Chapter 4 discusses characterization techniques and their results. Chapter 5 discusses these results and more general considerations. Finally, Chapter 6 gives overall conclusions with recommendations.

# Chapter 2

# Titanium Nitride

## 2.1 General Properties

Titanium nitride (TiN) is a refractory interstitial nitride with a golden color, extreme hardness, corrosion resistance, and relatively high conductivity. (Some properties of TiN [6] [9] [10] have been summarized in table 2.1 and compared to those of Ti.) Though several phases exist (see table 2.2 and fig. 2-1), the primary nitride phase, TiN, crystallizes in the rocksalt structure (Fm$\bar{3}$m) with a lattice parameter of 4.24Å for the stoichiometric material. The close packed structure, an fcc Ti sub-lattice with N filling all octahedral sites, is due to the relatively small size of the N atoms compared to Ti (0.74Å vs. 1.47Å). In order to accommodate the interstitial nitrogen, Ti must transform from a bcc or hcp structure to fcc, and $N_2$ must decompose to atomic nitrogen ($N_2 \rightleftharpoons 2N,\ \ \Delta H_o = 943.8$kJ/mol). The fcc structure of TiN follows readily from Hägg's rules [11] for structures (based on ionic radius ratios of Ti and N) and Pauling's rules [12]. The rocksalt structure of TiN (*cf.* hcp or bcc for Ti) is also indicative of an increase in the number of valence electrons from Ti to TiN, according to the Engel-Brewer theory [10] (which ranks various structures based on the number of sp-type electrons per atom). Clearly, this suggests that N is responsible for the increase in valence electrons. This is borne out to some degree when comparing the density of states for fcc-Ti and TiN, which does show an increase the sp density of states from fcc-Ti to TiN [13] [10]. Bonding is thus predominantly metallic, but with

some covalent and ionic contributions as well. The largely metallic nature of TiN is also clearly shown by the TiN band structure [13], shown in fig. 2-2. Metallic bonding is a general characteristic of the interstitial nitrides (such as Ti, V, Zr, Nb, Hf, and Ta nitrides), which all exhibit high electrical and thermal conductivity, in addition to high melting temperatures, high hardness, and chemical resistance. TiN is isomorphous with TiC, $TiO_x$ and other interstitial nitrides and carbides, forming complete solid solutions [9].

$Ti_2N$, the other major Ti-N compound [14], has two known phases, $\epsilon$-$Ti_2N$ and $\delta'$-$Ti_2N$ [14] [15]. The $\epsilon$-$Ti_2N$ phase crystallizes in the "anti-rutile" ($P4_2/mnm$) structure at temperatures below 900°C, which consists of an bcc Ti lattice, with N atoms filling one-half of the available octahedral sites (rather than all of the octahedral sites as in TiN) [12] [14]. The unit cell is tetragonal (unit cell $2Ti_2N$), with a=4.945Å and c=3.034Å [15]. The $\delta'$-$Ti_2N$ phase, essentially a vacancy-ordered form of the rocksalt structure with a small tetragonal distortion, has a resulting symmetry $I4_1/amd$, and a nitrogen fraction of ~38 at.% [14] [17]. Thus, as N is added to Ti, Ti transforms from the hcp $\alpha$-Ti phase to the bcc $\epsilon$-$Ti_2N$ phase, and finally to the to fcc $\delta'$-$Ti_2N$ and $\delta$-TiN phases, as expected by the Engel-Brewer theory. Again, this also suggests that as the N fraction increases, the number of valence electrons increases. The color of the $Ti_2N$ phases have been reported as a bright yellow [2], as opposed to the golden yellow for TiN.

Little is known about the electronic or mechanical properties of the $\epsilon$ and $\delta'$ phases, and even less of the other sub-stoichiometric Ti-N phases (see table 2.2). However, due to the large number of N vacancies in both phases of $Ti_2N$, one may suspect that the electronic properties will be quite adversely affected. There is some indirect evidence to this effect. Since TiN and TiC are quite similar (as are most of the interstitial nitrides and carbides), with the same crystal structure and similar electronic properties, one may possibly infer the general behavior of substoichiometric TiN phases from substoichiometric TiC. The resistivity of $TiC_{1-x}$ show a minimum for x=0 (*i.e.*,

| Property | TiN | Ti |
|---|---|---|
| Structure | fcc (NaCl) | hcp |
| Space Group | $Fm\bar{3}m$ | $P6_3/mmc$ |
| Range of Composition | $TiN_{0.6-1.1}$ | N/A |
| Color | Golden | Grey |
| Density | 5.40 g/cm$^3$ | 4.54 g/cm$^3$ |
| Melting Point | 2950°C | 1940 °C |
| Specific Heat | 37.0 J/mol · K | 25.0 J/mol · K |
| Thermal Conductivity | 30 Watt/m·K | 13 Watt/m·K |
| Thermal Expansion | 9.36x10$^{-6}$/K | 11x10$^{-6}$/K |
| Electrical Resistivity (bulk) | 20 ± 10 $\mu\Omega$·cm | 39 $\mu\Omega$·cm |
| Hall constant | -6.7x10$^{11}$m$^3$/C | -7.7x10$^{11}$m$^3$/C |
| Vickers Hardness | 21-24 GPa | 0.55-2.5 GPa |
| Modulus of Elasticity | 612 GPa | 110 GPa |
| Young's Modulus | 590 GPa | 120 GPa |

Table 2.1: Properties of Ti and TiN, at Room Temperature
(Compiled from [9] [10] [15])

stoichiometric) and a strong increase in resistivity as x decreases [15]. One may expect the same behavior for $TiN_{1-x}$, as has been reported by a few researchers [16], showing a general increase in resistivity with decreasing nitrogen fraction. The $Ti_2N$ phases should behave in the same manner as substoichiometric rocksalt TiN, given that the $\epsilon$ and $\delta'$ phases are rocksalt derivatives, but even more extreme. This will be discussed more in Chapter 5.

As with the interstitial carbides, the interstitial nitrides are stable over wide compositional ranges, generally with extensive vacancy concentrations on nonmetal sites, and to a lesser extent on metal sites. Generally, N vacancies are seen predominantly for nitrogen fractions less than 1, while Ti vacancies are seen predominantly for nitrogen fractions greater than 1 [15]. TiN in the rocksalt structure tolerates a nitrogen fraction of ~0.6-1.16 [9], and is primarily non-stoichiometric. Even for "stoichiometric" TiN, large vacancy concentrations may exist on both sub-lattices. The large range of stable compositions for $\delta$-TiN leads to correspondingly large variations in external properties. For example, the lattice parameter and the hardness of TiN

| Phase | Structure | Space Group |
|---|---|---|
| $\alpha$-Ti | hcp | $P6_3/mmc$ |
| $\beta$-Ti | bcc | $Im\overline{3}m$ |
| $TiN^*_{0.26}$ | Hex. | – |
| $TiN^*_{0.30}$ | hcp | $P6_3/mmc$ |
| $\eta$-$Ti_3N_{2-x}$ | Rhomb. | R3m |
| $\zeta$-$Ti_4N_{3-x}$ | Rhomb. | R3m |
| $\epsilon$-$Ti_2N$ | Tetr. | $P4_2/mnm$ |
| $\delta'$-$Ti_2N$ | Tetr. | $I4_1/amd$ |
| $\delta$-TiN | fcc (NaCl) | $Fm\overline{3}m$ |

Table 2.2: Phases of Ti and $TiN_x$
(compiled from [9], [14], [15], [17].) (* Probably metastable.)

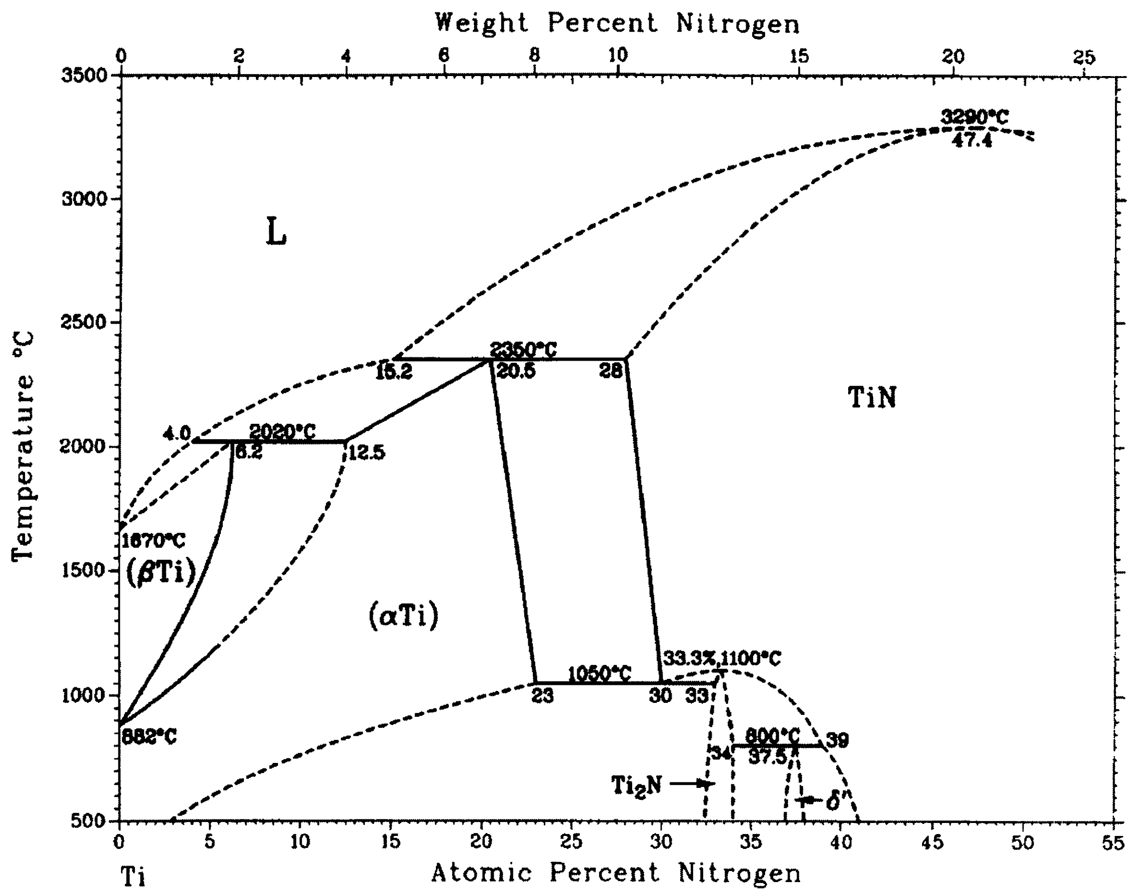


Figure 2-1: Ti-N Phase Diagram
(From [14].)

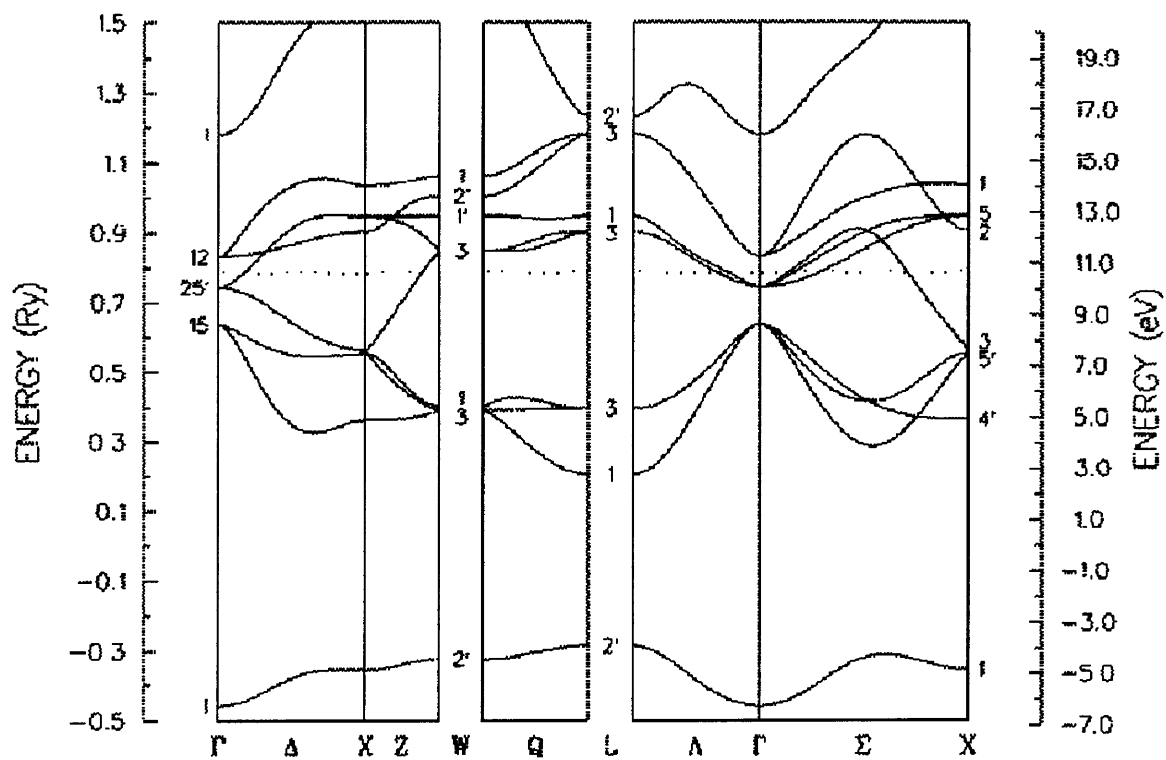


Figure 2-2: $\delta$-TiN (Fm$\overline{3}$m, a=4.24Å) Band Structure
(Dotted line is $E_f$. From [13].)

are observed to be maximal for stoichiometric TiN (see figure 2-3) [15]. The color of TiN also varies strongly with composition; with increasing nitrogen content the color changes from a titanium grey to light yellow ($Ti_2N$) to golden (TiN) to brown to bronze, and finally red [2] [6], with the presence of $H_2O$ or $O_2$ adding a purple hue [4]. Such variations of color and other properties with composition implies that when composition may not be directly measured (*e.g.* Auger analysis of TiN is difficult due to an overlap of Ti and N peaks [18]), external properties such as lattice parameter (see fig. 2-3) and color may be used to get a rough idea of composition, though care must be taken to account for other possible variations in these external properties (*e.g.* $H_2O$ present will alter color, and internal stress will alter the lattice parameter). Varying nitrogen content of the samples can also cause the introduction of substoichiometric Ti-N phases, leading to a wide range of microstructures. For example, sub-stoichiometric phases or pure Ti may appear in the bulk or at grain boundaries [19], which obviously alters mechanical properties, resistivity, and many other properties.

The properties of TiN are extremely sensitive not only to nitrogen fraction, but to impurities as well, especially oxygen. Controlling oxygen content is of extreme importance, since the free energy of formation for titanium oxides are much more favorable than for TiN [20] [21] (see table 2.3), and some amount of undesirable titanium oxides may form even with a small amount of oxygen present. Oxygen presence alone has been shown to adversely affect many properties, including conductivity, hardness, film adhesion, as well as optical properties, to name a few. Other impurities, such as water vapor, can cause similar problems. Thus, it is of key importance that some attempt be made to determine what nitride phases and impurities are present (at the very least), if not overal composition and microstructure as well. The presence or absence of non-primary phases and variation of microstructure considerably alters nearly any property in question.

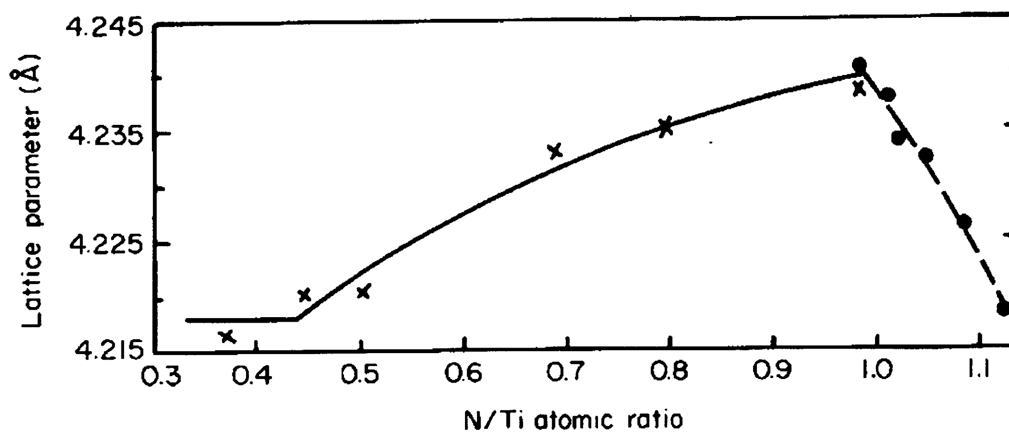


Figure 2-3: Lattice Parameter vs. Composition for $TiN_x$
(Adapted from [15].)

| Compound | $\Delta H_f^\circ$ (kJ/mol) | S° (J/mol-K) |
|---|---|---|
| TiN | -337.7 | 30.31 |
| TiO | -542.7 | 34.8 |
| $TiO_2$ | -849.1 | 72.32 |
| $Ti_2O_3$ | -1521 | 77.25 |
| $SiO_2$* | -910 | 41.5 |
| $Si_3N_4$ | -745 | 113 |

Table 2.3: Enthalpies and Entropies of Formation at 298K for Selected Compounds
(From [20], [21]. * Vitreous.)

# Chapter 3

# Preparation

## 3.1 Enhanced Activated Reactive Evaporation

Enhanced activated reactive evaporation, or EARE, is based on activated reactive evaporation (ARE), developed by Bunshah and Raghuram [22] in 1972. The ARE process is a hybrid process using reactive evaporation, but with the augmentation of energetic electron bombardment. In the original ARE design, which utilized an electron beam evaporation source, a positively biased probe draws electrons from the molten pool into the reaction zone between the source and the substrate. The electrons serve to activate the metal vapor and the reactive gas, thus increasing the reaction yield. The electron beam thus heats the metal source and supplies electrons for activation of reacting species. Due to the high electron flux, a plasma is maintained near the reaction zone. Advantages of this process include: 1) greatly improved reaction kinetics; 2) control of chemical composition, by changing the ratio of reactive gas and metal vapor species; 3) synthesis of high melting point compounds; 4) independent control over film growth and compound formation, unlike CVD methods; and 5) potential for synthesis of compounds which may not form in normal reactive evaporation [8]. However, in this design, there are several problems. Electron beam power decreases for decreasing deposition rate, and the supply of electrons which are used for activation becomes insufficient at low rates. Thus, low deposition rates are difficult to achieve. This also serves to couple the deposition rate, gas pressure, and

electron current, effectively eliminating independent control of these parameters.

The problems with the ARE process were essentially solved through a modification by Yoshihara and Mori [8], which added a separate electron emitting electrode to independently control electron and metal vapor flux. This not only decoupled the evaporation rate and electron current, but allows the use of non-$e^-$ beam deposition sources (*e.g.*, resistive sources ). This process is known as "enhanced" ARE, since it allows independent evaporation and electron source controls, greater control over reactive gas pressure, as well as extremely high deposition rates (up to several thousand Å/s possible). However, remaining problems are: 1) severe substrate heating due to plasma discharge; 2) additional sample heating due to the deposition source (typically at very high deposition rates); and 3) strong ion bombardment, which can lead to severe etching of both substrate and film. The first and second can be somewhat solved by system geometry, decreasing deposition time, or decreasing deposition rate. The third can be controlled by substrate and anode bias, but often remains a problem.

## 3.2 Electron Shower

The "electron shower" (ES) method by Yumoto *et. al.* [7] is a slight modification of the EARE process, which adds a pre-deposition activation of the substrate surface. This pre-deposition activation serves to make the substrate surface highly reactive, and promote substrate-reactive gas reactions leading to chemical anchoring mechanisms. Some additional advantages of the ES process observed include lower background gas inclusion, improved mechanical properties, improved adhesion, and, in the case of indium tin oxide (ITO) transparent conductors, improved conductivity was observed [23]. To date, EARE/ES processes have been used to prepare a wide variety of compounds, including: TiN, $Y_2O_3$, TiC, ZrC, HfC, VC, NbC, TaC, AlN, and $InSbO_x$, with greatly improved properties noted in many cases. The primary departure from EARE is the lack of a plasma discharge in the reaction volume, in

general much lower deposition rates (~1Å/s), and the use of a ring anode in place of the simple wire probe used in ARE or EARE. Excessive heating is less of a problem, with the lack of a plasma discharge and much lower deposition rates. The ES process can also aid in non-reactive deposition; it has been shown, *e.g.*, that it improves the adhesion and hardness of Cu films on stainless steel [7]. In the case of reactive deposition, the ES process cannot sustain very high deposition rates compared to EARE typically, primarily due to the lack of reactant volume ionization (as opposed to surface ionization) and slower kinetics. These seemingly small departures from EARE can have significant implications, however, some of which we will discuss shortly.

## 3.3 ES/EARE Apparatus and Procedure

Figure 3-1 shows a schematic of the experimental apparatus used, which is similar to the apparatus in reference [7]. As will be described below, this apparatus can be used to fabricate reactivly evaporated, ES, or EARE samples. A Ta sheet metal self-resistive source (henceforth "boat") was used to evaporate Ti metal and thus provide a flux of Ti atoms in the reaction zone. Ti deposition is monitored by a calibrated quartz crystal monitor directly over the source, with a relative accuracy typically of ~10%. The crystal monitor is positioned above the substrate level and out of the reaction zone to monitor *only* Ti deposition. For EARE samples, it was found that the crystal monitor could not be used with reasonable accuracy due to the presence of the plasma discharge, and was found to be accurate to only 25-50% in that case. Directly above the Ti source, an electrically isolated Cu substrate heater block is attached to a substrate arm which pivots to allow movement between the reaction zone and a shield (effectively blocking deposition; not shown in fig. 3-1). Substrates of high quality glass or Si(100) were affixed to the underside of the Cu block with Ag conductive paint [24], and a chromel-alumel thermocouple was attached to the block near the substrates to monitor the temperature. Near the Ti source was a W wire wound filament, which was resistively heated to provide thermal electrons. A

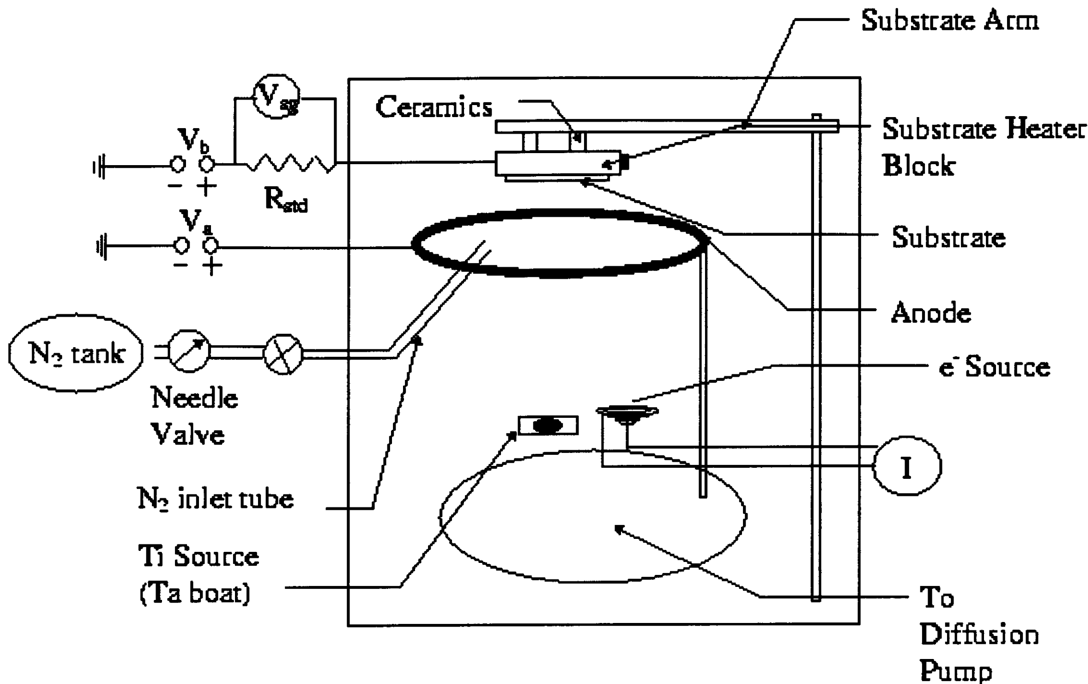


Figure 3-1: Electron Shower/EARE Apparatus.
($V_a$=$e^-$ acceleration voltage, $V_b$=substrate bias, $V_{sg}/R_{std}$=$e^-$ current between substrate and ground.)

ring shaped anode ($V_a$ = 0 - 1500V) accelerated the thermal electrons toward the substrate, which could also be biased ($V_b$ = 0 - 500V). A needle valve provides the necessary flow of ultra high purity $N_2$ gas into the reaction zone near the substrate (0.5-5cm away). Typical $N_2$ pressures in the bulk of the chamber were $\sim 10^{-4}$ torr. Base pressure in the vacuum system was approximately 7x$10^{-7}$ torr. Table 3.1 lists process parameters for both ES and EARE methods with descriptions and typical values.

Thermal electron generation was monitored by measuring current between the positively biased substrate ($V_b$ and ground. In addition, leakage current between

| Symbol | Parameter | Typical ES | Typical EARE |
|---|---|---|---|
| $P_{N_2}$ | Nitrogen pressure* | $\sim 10^{-4}$ torr | $\sim 10^{-4}$ torr |
| $t_{Ti}$ | Ti thickness | 200-2000Å | 500-2000Å |
| $\dot{t}_{Ti}$ | Ti deposition rate | <0.5-4Å/s | 2-200+ Å/s |
| $V_b$ | Substrate bias | 0-100V | 0-500V |
| $V_a$ | Anode bias | 0-1500V | 0-100V |
| $T_s$ | Substrate temperature | RT-500°C | 200-500°C |
| $I_{sg}$ | Substrate-Ground Current | 0-50mA | 100-600mA |

Table 3.1: Process Parameters
(* "Equilibrium" pressure in bulk of chamber.)

the substrate block and substrate arm, and background current (occuring when substrate and anode were biased without heating the electron source) were monitored and found to be negligible. Since the electron source and Ti source are grounded, as is the vacuum system, this effectively measures the current due to thermally generated electrons bombarding the substrate, $I_{sg}$ (after subtracting leakage and background). Typical values of $I_{sg}$ were ~0-50mA for the ES method, and 100-600mA for the EARE method. The electron bombardment, or "activation" serves to ionize both $N_2$ and Ti atoms within the reaction zone, as well as enhancing the reactivity of the substrate surface.

After mounting substrates (typically 2 glass and 1 Si(100)), the experimental procedure for ES samples is as follows: a) the vacuum chamber is pumped to its base pressure; b) the heater is warmed to a stable temperature, and outgassed along with the electron source and Ti source; c) $N_2$ lines are flushed, and a steady flow of $N_2$ is established with the needle valve; d) substrate and anode are biased; e) the electron source is heated; f) the substrate arm is moved into the reaction zone, and bombarded with electrons for 3-5min ("activation" phase); g) near the end of activation, the Ti source is slowly ramped until deposition occurs; h) once deposition is complete, the substrate arm is moved out of the reaction zone. Electron current ($I_{sg}$) is monitored both during activation and during deposition. EARE samples differ in that steps f), and g) involve a plasma discharge in the reaction volume, and typically much higher

deposition rates are used. It was observed that for ES samples, the upper limit of the deposition rate for significant TiN formation was ~5Å/s, while for EARE no limit was seen up to deposition rates of ~300Å/s (the highest easily sustainable and controllable with the thermal source used).

Plasma generation in the reaction volume is controlled by $V_a$ and $V_b$. For low substrate biases (< 100V), a plasma discharge could be ignited by increasing $V_a$ past a critical "ignition" voltage (typically 50-100V for $V_b$=50-100V). Thus, in this case the process could be performed as ES (no discharge present), EARE (discharge present), or a combination of both. For high substrate biases (*e.g.* >50 V) a much lower $V_a$ was required for plasma ignition, and in some cases plasma was ignited for $V_a$=0. Modifications of the ES and EARE processes will be discussed below.

### 3.3.1 Modifications

Samples were prepared using standard ES and EARE methods; however, the typical process used has features in common with both ES and EARE methods. Like the ES method, a pre-deposition "activation" and substrate cleaning is used, either with electron bombardment and $N_2$ plasma or with electron bombardment only. Substrate bias is used for most samples ($V_b$ >0), as is the case for typical ES processes, but EARE seldomly uses substrate bias. The use of a grounded metal gas inlet tube helps maintain the plasma only where $N_2$ density is highest, *i.e.*, in the reaction volume near the substrate. Extent of the plasma is controlled by $N_2$ gas density, since the high electric field and high gas density requirements for discharge are met only in the gap between the inlet and the substrate. Plasma extent can also be controlled by controlling the $N_2$ gas flow rate (needle valve) or pumping speed (throttling) in addition to changing $V_a$ or $V_b$. EARE, which uses a discharge around a simple wire probe, does not lend itself to precise control over plasma location and intensity. Essentially, the plasma is only of use in the volume between the gas inlet and the substrate; the current modification ignites plasma in this region only and leads to much more effecient use of the

plasma. Ignition of the plasma is largely controlled by the anode, which focuses and accelerates the bombarding electrons into the substrate-inlet region. The electron bombardment and acceleration allows ignition at much lower pressures than typically achievable, compacts the design and reduces power required. Only $\sim$100V is needed to ignite a plasma for $\sim 10^{-4}$ torr chamber pressure, whereas tens of mTorr and up to or greater than 1kV are often required for typical glow discharge conditions. Further, much greater control can be exercised over conditions near the substrate, merely by adjusting the flow rate, throttling, or inlet-substrate distance. Plasma reactions and other aspects of reactive deposition are further discussed in Appendix A.

# Chapter 4

# Characterization and Results

## 4.1 X-ray Diffraction

### 4.1.1 Lattice Parameter

X-ray diffraction (XRD) was performed on most TiN samples, including those on glass and Si(100) substrates. Since prepared TiN films were typically 800-2500Å, a thin film attachment was used, fixing the incidence angle ($\theta$). Scans were performed over $2\theta$=30-95° in most cases. Figures 4-1 to 4-4 show a few representative XRD patterns. Other XRD patterns can be found in Appendix B.

XRD data indicate that all samples analyzed contained TiN in the Fm3m structure. Peak positions corelated well with the TiN powder diffraction file (PDF 38-1420). Lattice parameters were calculated from the patterns using the strongest peaks, and generally agreed well with the TiN standard (see table 4.1). Since lattice parameter is known to vary with composition [15], calculated lattice parameters can give some estimate of the composition (see fig. 2-3), but only roughly if internal stress is not taken into account. However, the range of accuracy required for a crude estimate of composition from XRD data, even considering internal stress, is at least ±0.005Å, which is evident from fig. 2-3. In the present case, lattice parameter determination was generally no better than ±0.005Å, and in some cases was as high

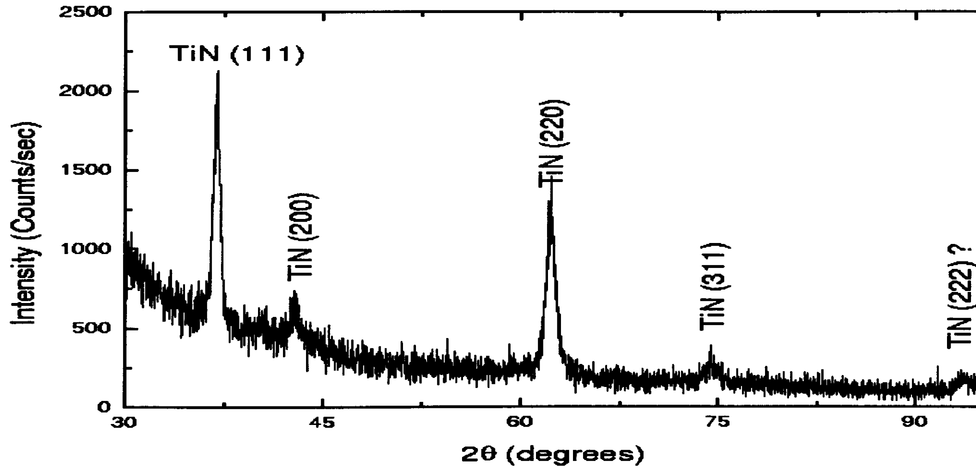


Figure 4-1: X-ray Diffraction Pattern for 9-207.
(Glass substrate, ES process. Note near absence of (200) peak.)

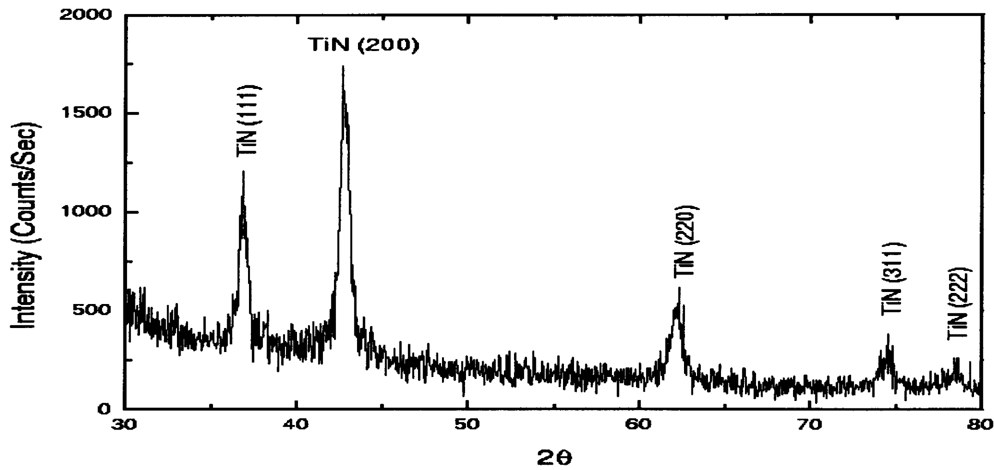


Figure 4-2: X-ray Diffraction Pattern for 9-210.
(Glass Substrate, EARE process. Note dominance of (200) peak.)

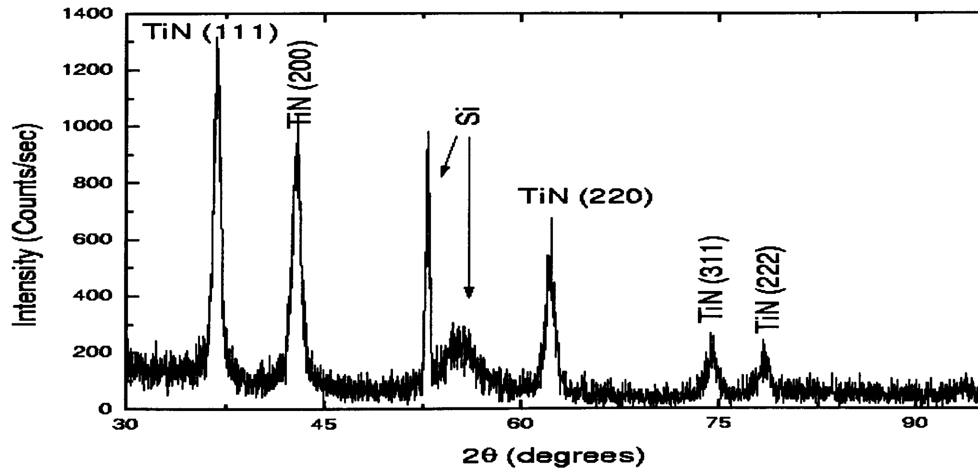


Figure 4-3: X-ray Diffraction Pattern for 9-210.
(Si(100) substrate, EARE process. Slight (111) prevalence.)

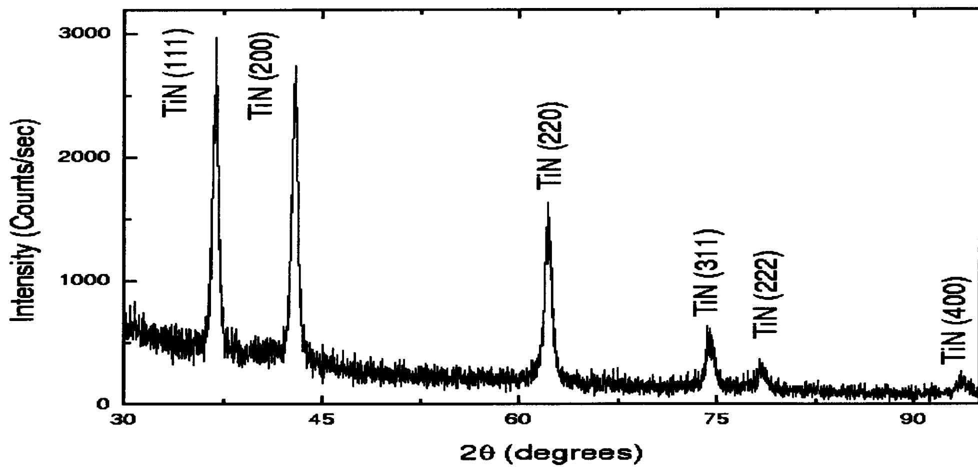


Figure 4-4: X-ray Diffraction Pattern for 9-213.
(Glass substrate, EARE process. (111) and (200) near equal intensity.)

| Sample | a (Å) |
|---|---|
| PDF 38-1420 | 4.2417 |
| 9-182 G | 4.223 ± 0.006 |
| 9-186 G | 4.15 ± 0.02 |
| 9-195 G | 4.236 ± 0.012 |
| 9-201 G | 4.212 ± 0.02 |
| 9-207 G | 4.219 ± 0.01 |
| 9-210 Si | 4.225 ± 0.01 |
| 9-210 G | 4.223 ± 0.01 |
| 9-212 Si | 4.224 ± 0.004 |
| 9-212 G | 4.221 ± 0.002 |
| 9-213 Si | 4.220 ± 0.004 |
| 9-213 G | 4.220 ± 0.006 |

†G refers to glass substrate, Si refers to Si(100) substrate.

Table 4.1: Calculated Lattice Parameters

as ±0.02Å. Thus, in the present case, one can only determine that the composition is indeed within the tolerated range for $\delta$-TiN (*i.e.*, $TiN_{0.6}$-$TiN_{1.1}$). Table 4.1 lists calculated lattice parameters for some samples, along with the TiN standard. Listed accuracy is only mathematical, and should not be given any undue physical significance. Chapter 5 will discuss these problems in more detail.

### 4.1.2 Crystallinity, Other Phases Present

Crystallinity of ES samples decreased considerably for lower substrate temperatures. EARE samples showed little such dependence; reasons for this will be discussed in Chapter 5. Most samples did not show evidence of sub-stoichiometric (*e.g.* $Ti_2N$) or other (*e.g.* $TiO_x$) phases in the XRD patterns. However, a few samples showed peaks which were not due to TiN alone. Sample 9-201 (see Appendix B) showed the presence of 2 peaks most likely due to $\alpha$- or $\beta$-Ti and $\delta'$-$Ti_2N$; 9-212(glass) (see Appendix B) also showed the possible presence of additional peaks. However, in the latter case the peaks observed were scarcely above the background intensity, and their position (or existance) cannot be determined with any accuracy. Sample 9-213(glass) (see fig. 4-4)

shows a small peak possibly from $\alpha$- or $\beta$-Ti; however, a sample from the same process on Si(100) (9-213 Si) shows no such peak. Sample 9-211(glass) showed at least 7 peaks which were not due to TiN. Most of these peaks can be accounted for by $\alpha, \beta$-Ti, or $Ti_2N$ phases. Due to the many peak overlaps of the substoichiometric TiN phases, exactly *which* phase is present is uncertain. However, the presence of a substoichiometric phase or combinations of various phases is substantiated, although small, for these few samples. These phases can account for all but 2 peaks, at $2\theta$=47-48°, which are tentatively attributed to Ti oxides. Chapter 5 will clarify further which phases are likely to be present, based on the Ti-N phase diagram and known processing variables.

### 4.1.3 Peak Heights

All but a few samples examined showed predominance of the (111) TiN peak, with the (200) and (220) peaks being second and third most prominently, respectively. In some cases, the (200) peak was almost totally supressed. However, two samples showed (200) predominance, while other samples showed strong (200) suppression. Typically, 5-6 TiN peaks could be observed, corresponding to (111), (200), (220), (311), (222), and (400) planes. However, only the (111), (200), and (220) peaks were ususally of significant intensity. Figure 4-5 shows background corrected peak intensity ratios ($I_{(111)}/I_{(200)}$) for some samples. In general, samples deposited on Si(100) had a larger (111)/(200) intensity ratio; in other words, samples on Si(100) showed stronger (111) orientation than those of the same process on glass. All samples where (200) orientation was favored were those on glass; samples from the same process on Si(100) favored (111) orientation. PDF data for TiN indicates that the (111)/(200) ratio should be 0.6-0.7, as is nearly the case for 9-186(glass) and 9-210(glass). All other samples thus show favored (111) orientation to some degree, with respect to the PDF standard.

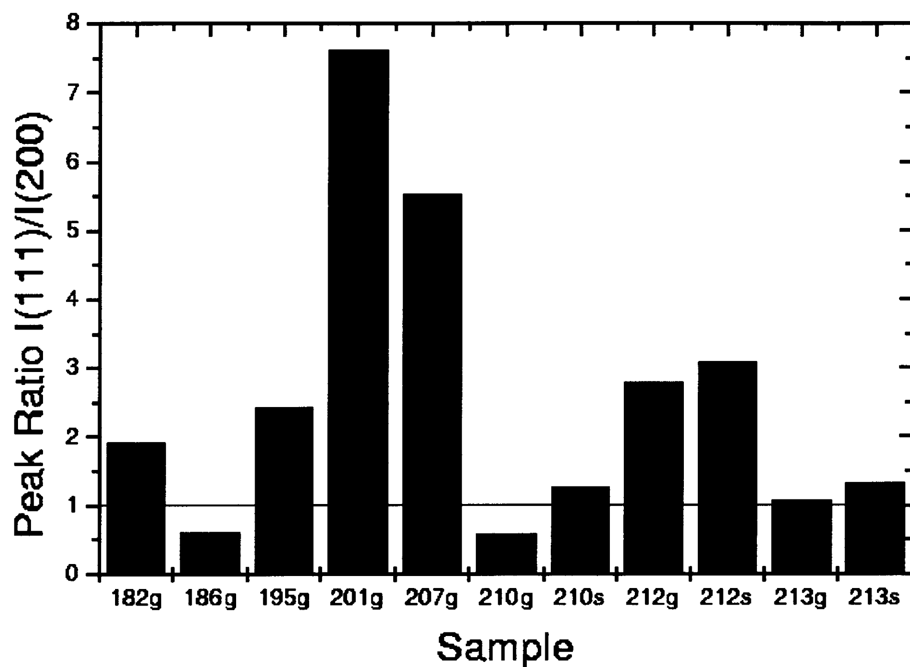


Figure 4-5: XRD (111)/(200) Peak Intensity Ratios for Prepared Samples. (Ratio is 0.6-0.7 for TiN standard (PDF 38-1420). Samples 210, 212, 213 are EARE; remaining are ES.)

## 4.2 Atomic Force Microscopy

Atomic Force Microscopy (AFM) was utilized for two primary purposes: surface analysis, and measurement of film thickness. As discussed previously, the EARE process renders the crystal thickness monitor relatively inaccurate. To circumvent this, a small "dot" of Ag conducting paint was placed on one of the glass substrates prior to mounting for each process [24]. After careful drying and preheating of the substrate, the TiN films were deposited over the substrate and thus Ag paint. After deposition, the Ag paint was carefully washed away with isopropyl alcohol, leaving a sharp circular step. AFM was utilized to measure the step height, and thus sample thickness in several places.

### 4.2.1 Roughness and Grain Size

Surface analysis consisted of determining surface roughness and approximate average grain size, as well as looking for any larger scale features. In general, samples fabricated with the ES method, *i.e.*, without plasma discharge, were quite smooth with roughness ~20Å or less. Roughness in these samples increased with deposition temperature, as expected. Samples prepared by the EARE method, with plasma discharge, showed greater variation, with roughness from ~2-100Å, also generally increasing with deposition temperature. EARE roughness values were generally quite low considering that the deposition rates were quite high. For similar substrate temperatures, the roughness of EARE samples was similar or slightly higher than the roughness of ES samples. Grain size was in general smaller for EARE samples, when compared to ES samples of similar substrate temperature. Roughness *vs.* substrate temperature is plotted in fig. 4-7. Deposition rate showed no significant correlation with roughness or grain size in either case, but only a limited range of rates was used for either ES or EARE.

### 4.2.2 Grain Structure

For EARE samples, circular or ellipsoidal grains (when viewed normal to the substrate plane) were observed. Topography was indicative of columnar grain growth. Since no cross-sectional data could be obtained, determining grain structure in the growth direction (normal to the substrate plane) is quite difficult. However, sample 9-213 showed long filaments lying in the plane of the substrate at various angles, shown in fig. 4-6, indicating that the predominant growth mechanism was in fact columnar in that case. Another sample (9-216) showed columnar conglomerations growing at an oblique angle to the substrate, such that the columnar grains could be clearly observed (fig. 4-6. For larger grained samples (EARE only) which could be more clearly imaged, individual grains had hemispherical or elipsoidal domes, also showing evidence of columnar growth. Individual grains were often observed to cluster into larger conglomerations, with some grains growing together at grain boundaries. Thus, for EARE samples the representative grain structure appeared to consist of smaller subgrains, and larger conglomerations which grew in a columnar manner. It is unclear whether the individual grains also grow in a columnar manner, or whether it is only the conglomerations which do so.

For ES samples, spherical or elipsoidal domed grains were also seen, as well as some evidence of the columnar structure, though not nearly so clearly as for EARE samples. Based on AFM images, it is unlikely that these samples contain any large degree of ordering (columnar or otherwise) in the growth direction. Most ES samples showed very small grains (<600Å), some <100Å. In both EARE and ES samples, grain size generally increased with substrate temperature in a manner similar to roughness. Grain size *vs.* substrate temperature is plotted in fig. 4-7.

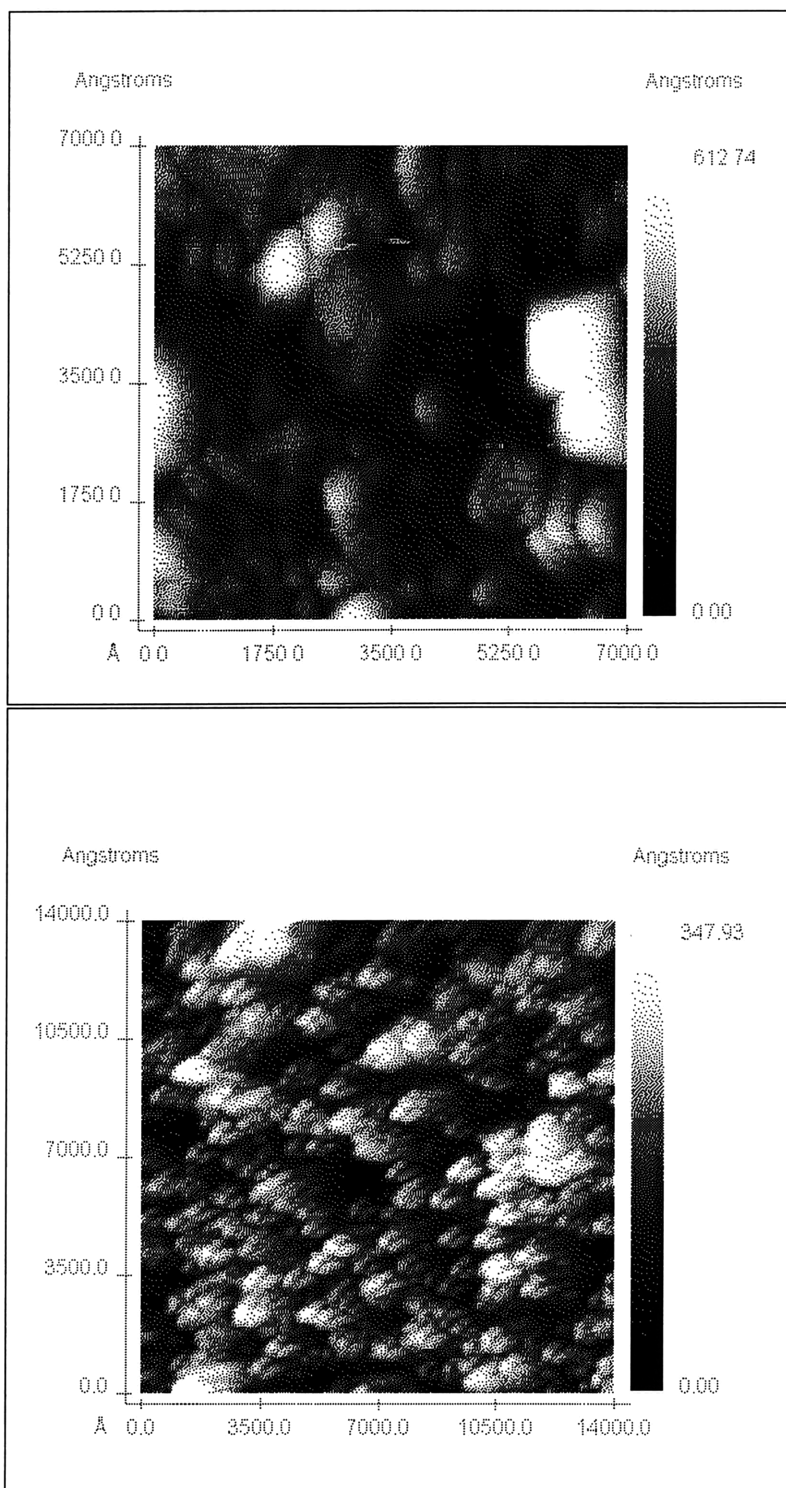


Figure 4-6: AFM Images.
A) 9-213; note filamentary structure. B) 9-216; columnar growth at an oblique angle, with sub-column grain structure.

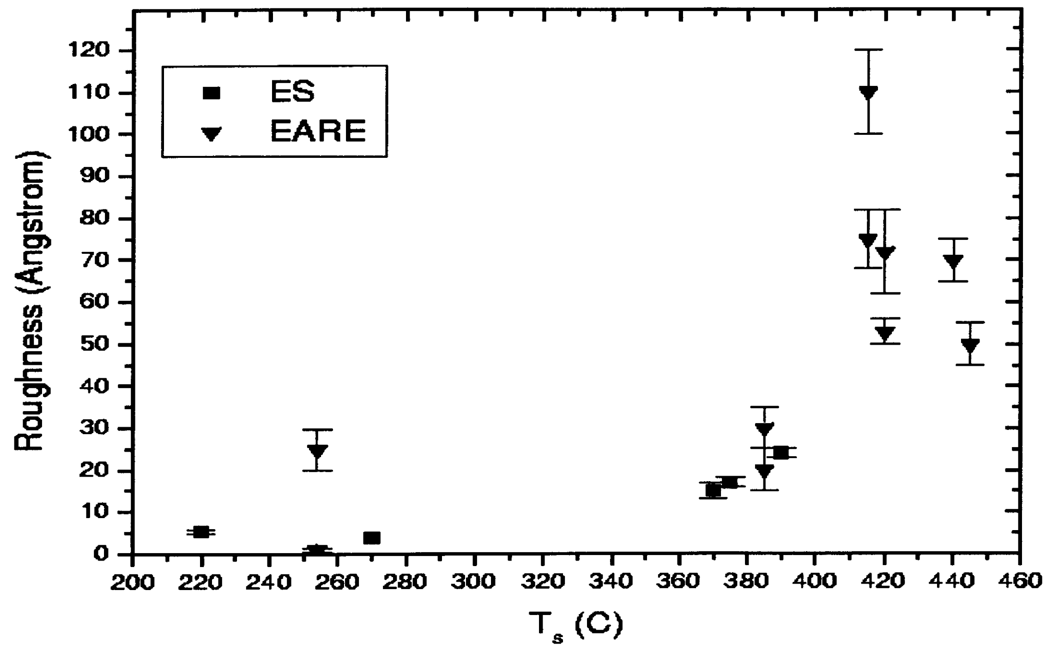


(A)

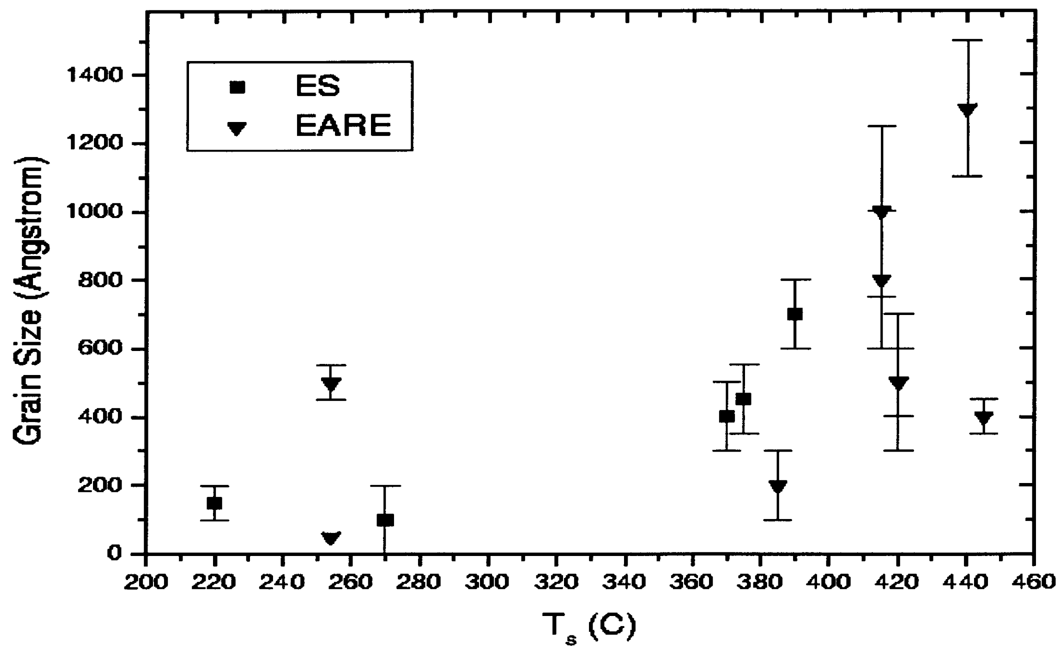


(B)

Figure 4-7: Roughness (A) and Grain Size (B) *vs.* substrate temperature.

## 4.3 UV-Visible-NIR Spectroscopy

Transmission and reflection data in the range of $\lambda$=300-2500nm were taken on a few selected samples. Since one application of TiN films is to provide infrared (IR; $\lambda$ >700nm) preferential reflectors, it is critical that samples with high reflectance in this range can be produced. Figure 4-8 shows transmission and reflection data for selected samples. In the near IR range (700-1000nm), reflectance as high as 50-60% was obtained for sample 9-211, and 40-50% for sample 9-213. From 1000-2500nm, reflectance increased an additional 10% in both samples. This is much better than typical samples prepared by the ES method [7], though lower than some samples prepared by sputtering [4] or Arc Ion Plating (AIP) [7]. However, reflectance data in the literature varies considerably, and the results obtained are well within the range of high-quality samples reported [2], and significantly better than many sputtered samples [26]. The increase of reflectance (or "knee") from 400-700nm is also quite pronounced, which is important for *preferential* reflection of IR. Reflection changes by a factor of ~3 over the range $\lambda$=400-700nm. Reflectance data also shows a plasmon edge at 375-400nm for both samples tested; this is indicative of metallic bonding [6]. Transmission was quite low, only ~5% for a 850Å sample, and <1% for samples of 1500-2000Å. Summing the reflection and transmission for samples examined indicates that at least ~20-30% of incident light is absorbed in the near-IR range. Thus, TiN films fabricated not only reflect IR radiation quite well, but also have a relatively large absorbtion coeficient for IR radiation, resulting in <1% transmission in most cases.

## 4.4 Resistivity vs. Temperature

Resistivity of the prepared TiN samples was examined using the four-terminal van der Pauw technique [25], which eliminates the influence of lead resistance. This is necessary in the present case due to the relatively low resistances (less than 1$\Omega$ to

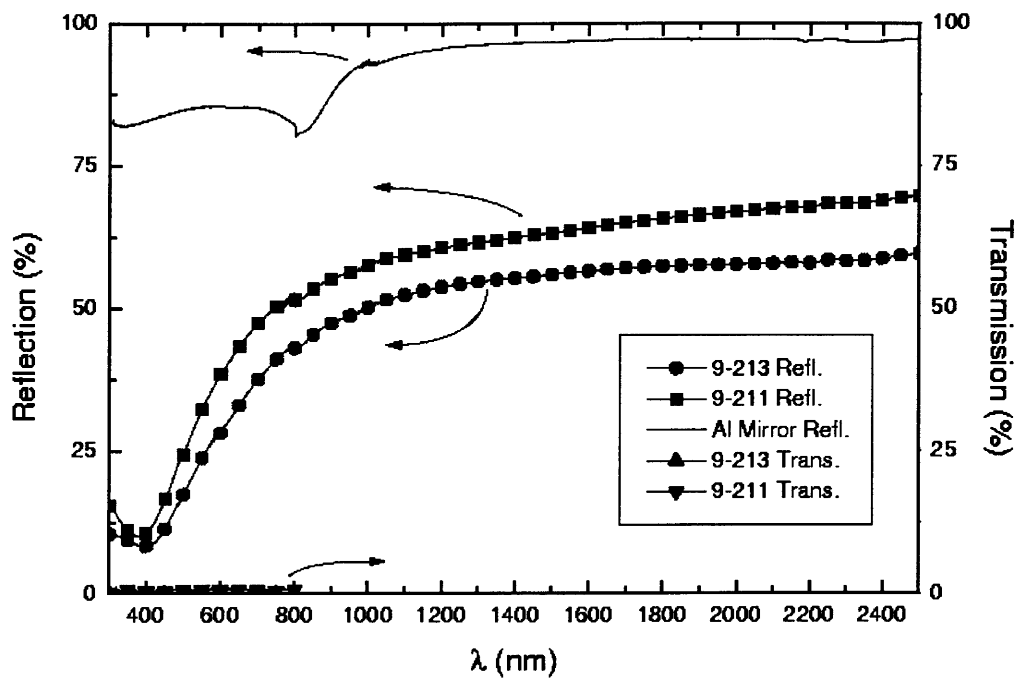


Figure 4-8: Reflection and Transmission *vs.* Wavelength. (Reflection data corrected for internal Al mirror.)

~100Ω) of the TiN samples. The van der Pauw technique has the added advantage of being independent of geometry, *i.e.*, only the sample thickness is needed to determine resistivity. Four terminal resistance were measured with an AC resistance bridge. Samples were mounted on a probe and slowly lowered into an insulated Dewar flask partially filled with liquid helium. Temperature, monitored with a silicon diode thermometer, slowly decreased as the sample was lowered. In this way, resistivity could be smoothly monitored as a function of temperature from 300K down to 4.2K. In order to test the accuracy of the measurement technique, a 550Å Au film was examined at 300K, comparing quite favorably with the bulk resistivity value.

Figure 4-9 shows a representative resistivity vs. temperature ($\rho$ vs. T) plots for prepared TiN samples (see Appendix C for other data). At room temperature, a wide range of resistivities is found, varying considerably with preparation conditions. The best samples showed a linear decrease in resistivity of 10-15% from 300K to ~50K, while some samples showed only a few percent decrease. A few samples exhibited an increase in resistivity with temperature. Samples exhibiting metallic behavior ($\rho$ decreasing with temperature) had resistivities in the range of 250-800$\mu\Omega$-cm. Below ~60K, all metallic samples showed a minima in resistivity between 35-55K, followed by a slight increase below the minima. This behavior will be explained in Chapter 5. In all cases, resistivity was much lower for samples prepared by the EARE method. Table 4.2 lists some of the resistivity vs. temperature results obtained, and table 4.3 lists bulk and other published data. The best prepared samples compare favorably with the some of the published values, but in general are relatively high. Possible reasons for this discrepancy will also be discussed in Chapter 5.

## 4.5 Post Deposition Annealing

Post process annealing was investigated for one of the TiN samples, 9-211G. A single sample on a glass substrate was cut into two pieces, and one was annealed in vacuum

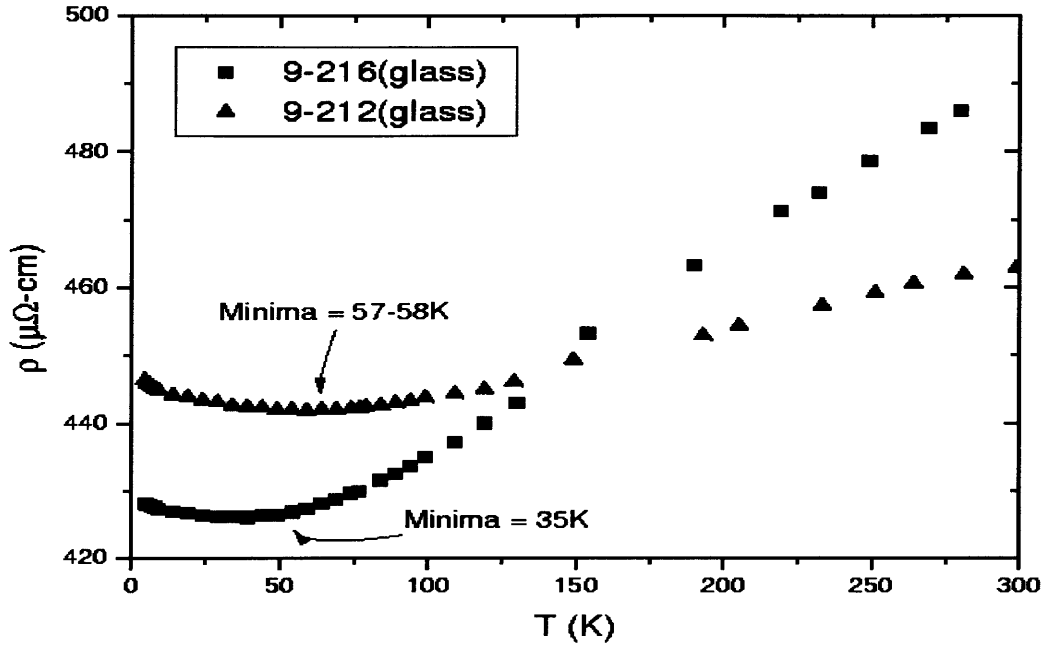


Figure 4-9: Resistivity *vs.* Temperature for 9-212 and 9-216

| **Sample** | $\rho_{300K}$ (**$\mu\Omega$-cm**) | $\rho_{77K}$ (**$\mu\Omega$-cm**) | $\rho_{4.2K}$ (**$\mu\Omega$-cm**) | $\rho$ *vs.* **T Behavior** |
|---:|---:|---:|---:|---:|
| 9-186 | ~3500 | ~75 000 | – | Semiconducting |
| 9-195 | 770 | 791 | 811 | Semiconducting |
| 9-201 | 2030 | 2620 | – | Semiconducting |
| 9-210 | 440 | 388 | 388 | Metallic |
| 9-211 | 262 | 252 | 253 | Metallic |
| 9-212 | 462 | 442 | 446 | Metallic |
| 9-213 | 570 | 537 | 540 | Metallic |
| 9-215b | 490 | 461 | 464 | Metallic |
| 9-215t | 667 | 661 | 671 | Metallic |
| 9-216 | 491 | 430 | 428 | Metallic |

Table 4.2: Resistivity of TiN samples on glass.

| Ref. | $\rho_{300K}$ ($\mu\Omega$-cm) | Type† |
|---|---|---|
| [26] | 75-200 | P |
| [27] | 20-100 | P |
| [28] | 50-100 | P |
| [29] | 18 | S |
| [29] | 90 | P |
| [2] | 100-625 | P |
| [30] | 75-300 | P |
| [31] | 40 | P |
| [9] [10] | 20±10 | Bulk |

†P denotes polycrystalline, S single crystal.

Table 4.3: Resistivity of reported TiN samples.

and the other in $N_2$ ambient. The vacuum annealed sample was heated to 450°C for 5.5 hours in a vacuum of 1x$10^{-6}$ torr, while the $N_2$ annealed sample was heated to 450°C for 5.25 hours in 2.3 torr of ultra-high purity $N_2$. Since both samples were smaller pieces of the same larger sample already characterized, they were identical before annealing, and any changes in external properties would be due to the annealing process only.

Several obvious changes were evident after the annealing process. The $N_2$ annealed sample had a slightly more brilliant golden color than an unannealed sample from the same process, and also appeared slightly more reflective. However, the vacuum annealed sample had a lighter, less golden top surface than an unannealed sample, while its back side appeared silver-grey, with almost no golden color. While both samples showed significant visual changes after annealing, the vacuum annealed sample displayed a much greater change in appearance than the $N_2$ annealed sample.

### 4.5.1 Effect on Resistivity

After the annealing and inspection, samples were mounted as described in section 4.4 and the resistivity was monitored as a function of temperature to 77K. Both annealed

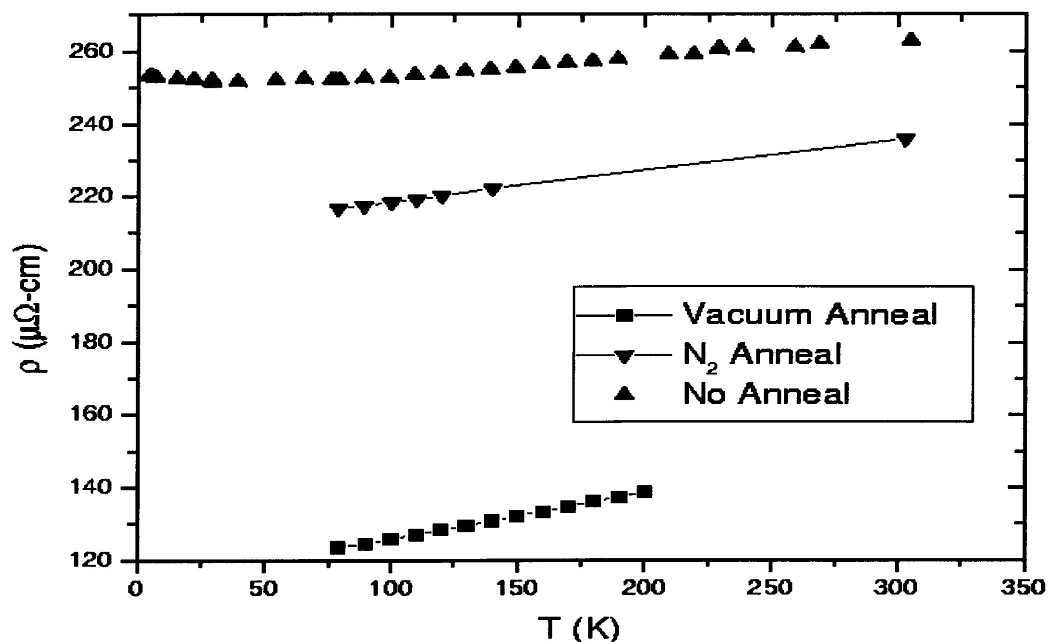


Figure 4-10: Effect of $N_2$ or vacuum annealing on resitivity *vs.* temperature behavior. (Sample 9-211)

samples were part of a larger sample already characterized in this manner; thus, resistivity changes could definitively be characterized. Resistivity *vs.* temperature for the unannealed, $N_2$ annealed, and vacuum annealed samples are displayed in figure 4-10. It is clear that annealing in either $N_2$ or vacuum decreases resistivity, and increases the temperature coefficient of resistivity. However, the effect is significantly stronger for the vacuum annealed sample. Possible reasons for this will be discussed in the next chapter.

### 4.5.2 Effect on Microstructure

The annealed TiN samples were also examined with AFM to determine changes in the microstructure of the films. Table 4.4 lists the roughness and grain size for 9-

| | Roughness* (Å) | Grain Size** (Å) |
|---|---|---|
| Unannealed | 14-17Å | ~100Å |
| $N_2$ Annealed | 6-8Å | 1000-1300Å |
| Vacuum Annealed | 8-10Å | 1100-1500Å |

Table 4.4: Effect of Vacuum or $N_2$ Annealing on Microstructure, 9-213G
(* Measured over a 14$\mu$m × 14$\mu$m area.)
(** Average grain size.)

213G before and after annealing. Both $N_2$ and vacuum annealed samples showed an increase in grain size of roughly an order of magnitude, and a decrease in small scale surface roughness. Though this is an expected phenomena [6], the magnitude of the changes may seem somewhat surprising given that the annealing temperature was quite low compared to the melting temperature of TiN (450°C *vs* ~3000°C). Reasons for the changes observed and their ultimate effects will be discussed in Chapter 5.

## 4.6 Adhesion

Though no highly quantitative adhesion tests were performed on these samples, several qualitative methods were utilized to give an indication of the relative adhesive strength of the TiN samples prepared on glass. The first of these, the canonical adhesive tape test, has been used and reported by many researchers and is thus of some utility for comparing the present work to previously reported work. This test consists of applying adhesive tape to the surface of the sample to be tested, and pulling the tape off at relatively fast and relatively slow rates. If the sample does not delaminate for fast or slow pull rates, it is judged "well adhered." If the sample does delaminate, the degree and nature of the delamination is noted. There are several difficulties in obtaining useful results from this method; perhaps the most obvious is that the type of tape used is seldom, if ever, reported. Despite these difficulties, the tape test indicates that prepared samples are "well adhered" to the substrate in some sense. Several TiN samples were examined in this manner, and none showed any degree of

delamination for a variety of adhesive tapes. This is particularly important, since some reported TiN samples have had poor adhesion to glass, showing a high degree of delamination, and in severe cases, peeling after exposure to air for several days [7].

A simple scratch test was also employed to gauge adhesive strength of the TiN films, as well as scratch resistance. A diamond scribe was used to scratch several TiN samples under quasi-constant loading. After scratching, and optical microscope was used to examine the scratched region for delamination or plastic deformation of the film. Adhesion of samples in this case was also found to be quite high, with the scratch test trace continuous from sample to substrate. No delamination was observed. For comparison, similar scratch tests were performed on evaporated Ti and Co films, which showed high plastic deformation and some degree of delamination in the region near the scratch for both films. Results were quite similar to those reported in [7]. These simple qualitative tests should not be taken too seriously, but more as a mere practical indication that the TiN films prepared are very stronly adhered to the substrate, especially when compared to typical evaporated metal films.

# Chapter 5

# Discussion

## 5.1 Apparatus Characteristics

The ES/EARE apparatus used in this work maintains the usual advantages of both of those methods. Either an ES or EARE process may be performed with the same equipment, or a combination of the two. Some of the more outstanding problems associated with these methods have been effectively dealt with as well. Substrate etching, sometimes a problem with the EARE process, is a function of the plasma intensity only, and can thus be controlled by controlling the plasma intensity. As outlined in Chapter 3, fine control over the plasma characteristics is one of the main features introduced in this work. However, some problems remain, such as substrate heating. This effect may be minimized by having a truly temperature controlled substrate holder (*i.e.*, with heating and cooling capacity). In addition, film uniformity over large areas has been a problem in the present case, due to the use of a simple tube gas inlet. This necessarily results in a unidirectional plasma. However, this problem is easily overcome *via* a simple modification of the gas inlet, which will be discussed in Chapter 6.

## 5.2 X-ray Diffraction

Lattice parameter data are generally consistent with near-stoichiometric TiN, but experimental error and the lack of internal stress data rules out any estimate of composition *via* XRD data. Even if internal stress were accounted for, the accuracy of lattice parameter measurements on the thin films measured is unlikely to be sufficient. Further, the accuracy of the published correlation [15] is quite uncertain, as no mention is made of correction for internal stress, method of composition measurement, *etc.* It may be clearly stated that the films produced are consistent with $\delta$-TiN, and that they probably are under compressive stress to some degree. However, composition is known only by the limits of the $\delta$ phase region. Previous work, as well as resistivity data (to be discussed), certainly suggest that these films may be substoichiometric to some degree, however.

Several samples showed some evidence of non-TiN phases. As discussed in Chapter 4, exactly which phases were present was not immediately obvious; peaks observed matched several candidate phases, including $\alpha$- and $\beta$-Ti, $\epsilon$- and $\delta'$-$Ti_2N$, and $TiN_{0.26}$. However, examination of the Ti-N phase diagram and other factors sheds some light. The Ti-N phase diagram indicates that if a Ti phase is present, it is likely to be $\alpha$-Ti [14]. The presence of $\beta$-Ti appears to be rather unlikely. Either $\epsilon$ or $\delta'$ $Ti_2N$ could be present, however. At the substrate temperatures used, the phase diagram indicates that only $\delta'$ may be formed with TiN. This neglects the increased surface temperature due to energetic particle bombardment, however, which essentially stimulates high temperature chemistry [33]. Thus, it cannot easily be determined from XRD data alone which of the two sub-stoichiometric nitrides is present.

XRD data also indicated that the orientation of the samples could be altered from (111) to (200). The alteration of preferred orientation by ion bombardment, deposition rate, and other factors has been reported by several researchers [34]. Generally, (111) oriented samples are seen, with some researchers reporting (200) or (220) ori-

entations. However, there is no general trend explaining the data; rather, it seems to vary from case to case on the specific preparation details. Figure 5-1 shows a plot of $I_{200}/I_{111}$ *vs.* substrate temperature for ES and EARE samples on glass and Si(100). The general trend indicates that at higher substrate temperatures, samples became more (111) oriented. For EARE samples, the effective surface temperature is almost certainly much higher than the substrate temperature due to the plasma discharge present; the same is true to a lesser degree for the ES samples. ES samples were also generally more (111) oriented than EARE samples, on the average. Some researchers have reported that increasing ion current altered preferred orientation from (111) to (200) [34]. Given that ion and electron current for EARE samples was at least two orders of magnitude higher than for ES samples, the orientation observed is generally consistent with the literature. However, a wide range of orientations were observed even for high ion-electron currents, indicating that substrate temperature and other parameters are also relevant. Though orientation can be changed from (111) to (200) in both ES and EARE methods, at present the parameters governing these changes are poorly understood. Substrate temperature appears to have the strongest effect of the parameters thusfar investigated, shown in figure 5-1.

## 5.3 UV-Visible-NIR

Though optical data appeared quite good, reflection was still somewhat low if IR reflection applications are to be considered (though perfectly adequate for other applications). However, optical measurements were performed under somewhat non-ideal circumstances. Samples used for these measurements had already been subjected to resistivity measurements, and had been stored and handled for nearly one month before optical measurements were performed. In order to get a true idea of the optical quality of films prepared by the ES/EARE method used here, films should be capped *in-situ* with a protective layer (which would not interfere with optical measurements) and measured as soon as possible after deposition. The process of making contacts

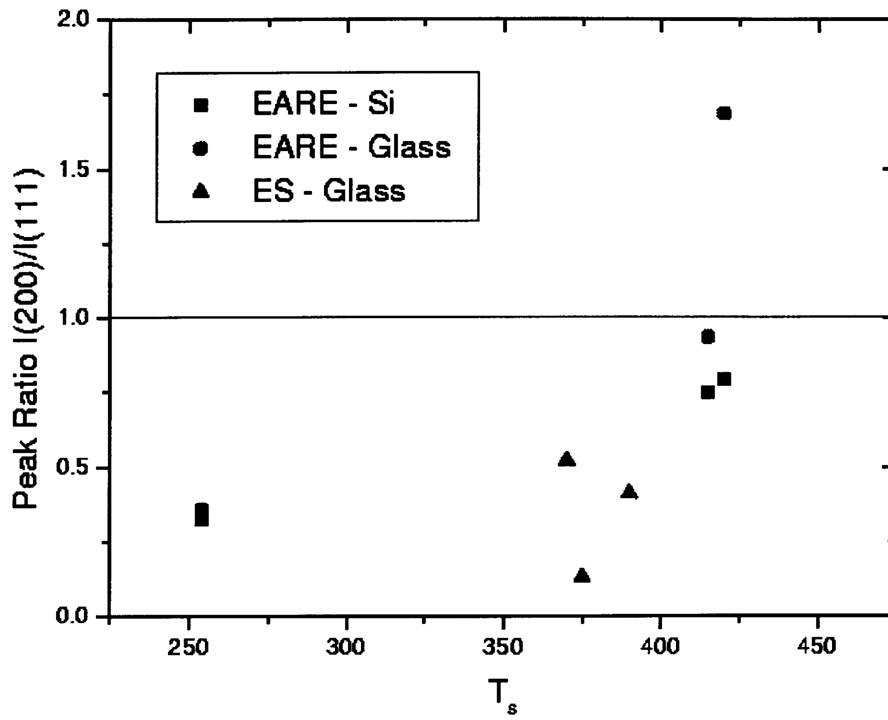


Figure 5-1: (200) to (111) Peak Ratio *vs.* Substrate Temperature.

for resistivity measurements, as well as handling and pre-cleaning for the optical measurements, certainly degraded optical properties of the films measured. Under better circumstances, reflection of films by the present method could prove substantially higher.

## 5.4 Atomic Force Microscopy

Roughness and grain size data are generally fairly good and reproducible. Grain structure data, though, must be more accurately determined. Since AFM gives only a surface view, any determination of the true grain structure in the absence of a cross-section involves some speculation. In spite of the lack of cross-sectional data, the surface data as well as growth conditions certainly suggest that the grains should be columnar [6]. In addition, it would be useful to determine whether or not the grains observed have subgranular structure below the resolution limit of the AFM used (lateral resolution ~50-100Å). The former problem could easily be remedied by cross-sectional TEM, or an AFM/STM analysis of a cleaved sample. The latter problem could be resolved with STM.

## 5.5 Resistivity *vs.* Temperature

Many questions are raised by the resistivity *vs.* temperature data. No superconducting behavior is seen for any samples examined, despite the fact that TiN has a $T_c$=5.6K [15]. The most likely explanation for the lack of an observable $T_c$ would probably be substoichiometry. The $T_c$ of TiN is known to be a strong function of the N/Ti ratio; $T_c$ may decrease to less than 4K (minimum temperature used in this work) for N/Ti~0.97 [15]. Thus, only a very small deviation from the correct stoichiometry would make the $T_c$ unobservable in the present case (measured down to 4.2K). This correlates well with previous studies of NbN films in this laboratory [32],

where was observed that the $T_c$ was a strong function of $N_2$ partial pressure for reactively sputtered NbN films. The variation of $T_c$ with the N/Nb ratio reported is similar, though much less drastic, to TiN [15].

Another somewhat unexpected feature of the resistivity behavior is magnitude of the room temperature resistivity. In the best case, resistivity was nearly one order of magnitude higher than the best reported TiN films or the bulk value. This can probably be best explained by a combination of two factors. First, resistivity of TiN has generally been reported as a strong function of nitrogen content [15] [16], though the degree of the variation is somewhat inconsistent. This is consistent with somewhat more detailed observations of the variation of resistivity and carrier concentration (*via* Hall measurements) with interstitial fraction for TiC, HfN, and other related compounds [15]. As the lack of superconductivity and previous work suggests, the films prepared are probably substoichiometric to some degree; only a small N deficiency may cause a relatively large increase in resistivity. In addition to stoichiometry, grain boundaries may play an important role in determining the overall resistivity. The TiN phase diagram indicates that $Ti_2N$ phases may segregate, possibly to grain boundaries. It is likely (see Chapter 2) that these phases are not good conductors, which would lead to a large grain boundary contribution, especially at low temperatures. More generally, the mere presence of grain boundaries at all can cause an increase in observed resistivity [6]; AFM data indicates that grain sizes are rather small for the prepared samples, which could lead to a large contribution to the resistivity. This is supported by the observations of Johansson *et. al.* [29], who reported that polycrystalline samples showed a resistivity more than three times higher in some cases when compared to similarly prepared single-crystal samples. Other researchers have also reported, in the case of reactive sputtering, that the minimum attainable resistivity was $\sim 200\mu\Omega$cm. In addition to these factors, it has also been observed that resistivity is a strong function of substrate bias for sputtered samples [2] [27], which may also be important in the present case.

Some of the speculation may be cleared up by the results of the annealing experiments. At the relatively low annealing temperatures used, the primary effect of annealing is most likely to increase nitrogen diffusion within the films. Films annealed in $N_2$ showed a more golden color, and lowered resistivity, which could be explained by N diffusion into substoichiometric films. This N diffusion into the films would bring the films closer to stoichiometry, and thus decrease resistivity [15]. This effect would be limited at the relatively low $N_2$ pressures used, and grain boundary effects would largely remain, which would explain the high resistivity even after annealing. Further annealing experiments at higher $N_2$ pressures and higher temperatures would help confirm this explanation.

Films annealed in vacuum also showed a decrease in resistivity. In that case, the back side of the film was almost devoid of nitrogen (grey color), while the surface showed a decreased presence of nitrogen (lighter golden yellow color). It is possible that at elevated temperatures in vacuum, N was able to diffuse out of the film. Further, the $SiO_2$ present in the glass substrates may cause displacement reaction with TiN to form Ti oxides, which would be more favorable at elevated temperatures. This would explain the larger nitrogen decrease at the glass-TiN interface. If N content were reduced sufficiently, the films would be primarily $\alpha$ or $\beta$-Ti with dissolved N (see fig. 2-1). Since $Ti_2N$ has a golden yellow color, the lighter color on the surface of the vacuum annealed films is consistent with a surface of $Ti_2N$, while the interface is consistent with $\alpha$ or $\beta$-Ti. Thus, these samples are indicative of a slight decrease of N content on the surface (TiN reduced to $Ti_2N$), and a further decrease at the film-substrate interface (TiN reduced to Ti). It is also reasonable that these films could have a lower resistivity than the pre-annealed substoichiometric TiN films, given the low resistivity of Ti. Again, further annealing experiments, as well as XRD analysis would be beneficial.

# Chapter 6

# Conclusions, Recommendations

## 6.1 Conclusion

High quality TiN films have been prepared by two novel methods: the electron shower process (ES), and Enhanced Activated Reactive Evaporation (EARE). Improvements have been made to the typical ES/EARE apparatus, including a more confined plasma geometry, better plasma control, and the combination of *both* ES and EARE methods in one apparatus. X-ray diffraction confirmed the correct NaCl structure for the films. TiN films prepared are extremely well adhered, quite hard, and show good electrical and optical properties. In addition, the process, with some refinements (see following section), is generally applicable to both reactive and non-reactive deposition where highly adhesive films are required with relativly low substrate temperatures.

## 6.2 Future Recommendations

The present work demonstrated the feasibility of preparing TiN films by the ES/EARE method. In order for this method to be more widely utilized, further work must be done, primarily in the areas of further apparatus optimization, and further sample characterization. If completed, both areas would yield a wealth of further information about the process itself, as well as how to prepare TiN films with specific properties.

One outstanding problem is the inability to coat large areas uniformly with the present apparatus. This may be easily remedied by replacing the simple tube gas inlet with a symmetric ring. Such a ring, with small outlet holes around its perimeter, would yield uniformity over much larger areas while maintaining the desired plasma confinement.

In order to more definitively determine the grain structure and composition of grain boundaries, we propose the following. STM may be utilized, along with cross-sectional TEM (or an equivalent method) to determine the grain structure with certainty. Scanning Auger spectroscopy may be performed on a ultra-high vacuum cleaved sample to determine the composition of grains as well as grain boundaries. With the small grain sizes as prepared, scanning Auger is most suitable due to its high spatial resolution. Resistivity *vs.* temperature measurements should be conducted at lower temperatures to determine if the films have an observable superconducting transition temperature, and X-ray photoelectron spectroscopy (XPS) or another method (*e.g.*, X-ray fluorescence, XRF) should be utilized to determine composition accurately. As mentioned, optical measurements on cleaner films should be performed. Finally, rigorous mechanical testing - including microhardness, adhesion, abrasion, and wear testing - should be performed. However, all of the further characterizations suggested would be most logically performed after the apparatus has been further optimized.

# Bibliography


[1] Many references exist; see, for example, R. Buhl, H.K. Pulker, and E. Moll, *Thin Solid Films* **80**, 265 (1981); R.L. Hatschek, *Am. Mach. Special Report* No. **752**, 129 March (1983).

[2] M. Wittmer, B. Studer, and H. Melchiar, *J. Appl. Phys.* **52**, 5722 (1981), *op. cit.*

[3] B. Zega, M. Kornmann, and J. Amiguet, *Thin Solid Films* **54**, 577 (1977)

[4] A. Mumtaz, W.H. Class, *J. Vac. Sci. Tech.*, **20**(3), 345 (1982)

[5] E. Valkonen, T. Karlsson, B. Karlsson, and B.O. Hojansson, *Proceedings of SPIE 1983 International Technical Conference* (1983) **401**, 41.

[6] M. Ohring, *The Materials Science of Thin Films*, (Academic, New York, 1992)

[7] H. Yumoto, K. Watanabe, K. Akashi, N. Igata, *Appl. Surf. Sci.*, **48/49**, 173-177 (1991)

[8] H. Yoshihara and H. Mori, *J. Vac. Sci. Tech.*, **16**(4), 1007 (1979)

[9] H.O. Pierson, *Handbook of Refractory Nitrides and Carbides*, (Noyes Publ., New York, 1996).

[10] S.T. Oyama, *The Chemistry of Transition Metal Carbides and Nitrides*, (Blackie Academic and Professional, New York, 1996)

[11] G. Hägg, *Z. Phys. Chem.*, **2**, 33 (1931)

[12] Chiang, Birnie, and Kingery, *Physical Ceramics*, (Wiley and Sons, New York, 1997), 37.

[13] D. Papaconstantopoulos, M. Keegan, B. Akdim, and C. Coley, *Electronic Structures Database*, http://cst-www.nrl.navy.mil

[14] T.B. Massalski, ed., *Binary Alloy Phase Diagrams*, vol. 3 (ASM Int'l, Materials Park, Ohio, 1990). pp. 2705-2707.

[15] L.E. Toth, *Transition Metal Carbides and Nitrides*, (Academic, New York, 1971).

[16] G.V. Samsonov, *Handbook of Refractory Compounds*, (Plenum, New York, 1980).

[17] A.N. Christensen, A. Alamo, J.P. Landesman, *Acta Cryst.* C**41**, 1009 (1985)

[18] Q. Zhang, *J. Vac. Sci. Tech. A* **13**(5), 2384 (1995)

[19] B. Jacobson, R. Nimmagadda, R. Bunshah, *Thin Solid Films* **63**, 333 1979

[20] J.A. Dean, *Lange's Handbook of Chemistry*, McGraw-Hill, New York, 1992

[21] National Institute of Standards and Technology, *NIST Chemistry Webbook*, http://webbook.nist.gov, No.69 (March 1998)

[22] R. F. Bunshah and A. C. Raghuram, *J. Vac. Sci. Tech.*, **9**(6), 1385 (1972)

[23] H. Yumoto, J. Hatano, T. Watanabe, K. Fujikawa, H. Sato, *Jpn. J. Appl. Phys.*, **32** pt. 1, No. 3A, pg. 1204 (1993)

[24] Previous work in this laboratory has shown that the Ag paint does not significantly contaminate samples, even at elevated temperatures.

[25] I.J. van der Pauw *Philips Research Reports*, **13**(1), 1 (1958)

[26] K.Y. Ahn, M. Wittmer, and C.Y. Ting, *Thin Solid Films*, **107**, 45 (1983)

[27] N. Kumar *et. al.*, *J. Vac. Sci. Tech. A*, **5**(4), 1778 (1987)

[28] Y. Massiani *et. al.*, *Thin Solid Films*, **191**, 305 (1990)

[29] B.O. Johansson *et. al.*, *J. Vac. Sci. Tech. A*, **3**(2), 303 (1985)

[30] D.S. Williams *et. al.*, *J. Vac. Sci. Tech. B*, **5**(6), 1723 (1987)

[31] T. Brat *et. al.*, *J. Vac. Sci. Tech. B*, **5**(6), 1741 (1987)

[32] J.S. Moodera, P. LeClair, and J. Fine, unpublished work (1992). Similar resistivty *vs.* temperature results were seen for a wide variety of NbN films.

[33] J.A. Thorton, *Thin Solid Films*, **107**, 3 (1983)

[34] J. Sundgren, *Thin Solid Films*, **128**, 21 (1985)

# Appendix A

# Reactive Deposition and Plasma Chemistry

## A.1 General Aspects of Reactive Deposition

The reaction of a metal vapor and a reactant gas (or another elemental vapor), in this case Ti and $N_2$, can take place at one or more of three locations: at the substrate, in the vapor region (volume between source and substrate), or at the vapor source (*i.e.* the Ti source). The latter is of little importance for the present case, and will not be considered. For all three of these locations, however, there are three vital factors which govern the reactions: sufficient supply of *all* reactants, collisions between reacting species, and reaction between colliding species [22].

Collision probability is governed by the mean free path , which is inversely proportional to the partial pressure ($\lambda_{mfp}(cm) = \frac{5x10^{-3}}{P(torr)}$) and also the source to substrate distance [6] If the source to substrate distance is smaller than the mean free path by a significant amount, essentially no collisions will take place in the vapor region. For example, if the source to substrate distance is 25cm, one would expect few volume collisions for $\lambda_{mfp} > 25$cm, corresponding to P < $2x10^{-4}$ Torr. If no collisions, and therefore no volume reactions, occur, the reaction proceeds only at the substrate surface. As the deposition rate increases, so must the supply of reacting species for

significant collisions to occur.

If the relevant reaction proceeds only at the substrate surface, the deposition rate must necessarily be limited. Each monolayer deposited must have sufficient time to react with the reactant gas (or vapor) before subsequent layers limit reactant diffusion greatly. If reactions are also proceeding in the vapor phase, as is the case for higher reactant pressures, this rate restriction is eased substantially. This indicates that for the highest possible deposition rates, it is essential that both surface and volume reactions occur. It then follows that high reactive deposition rates require high reactant pressures.

High pressures alone do not ensure high deposition rates, however. This is due to the fact that a collision does not assure a reaction. The details governing the probability of a reaction occuring are beyond the scope of this work. However, the probability for reaction may be increased substantially if one or both of the components is activated. This can be accomplished *via* microwave, UV, or electrical discharge (the present case), for example [22]. If a high reaction yield is required, activation of one of the components is often a requirement due to poor kinetics or unrealistically high deposition pressures. The former is particularly important for the case of nitride coatings, where free energies of formation, and thus reaction yields, are often quite low. The latter concern, high deposition pressures, is easy to understand in the case of thermal evaporation sources. Pressures in excess of 1mTorr may be required to instigate significant volume reactions for a particular experimental setup. Operating thermal sources at such a high pressure requires sometimes prohibitive amounts of power (vapor pressure increases strongly with increasing chamber pressure) or causes untolerable substrate heating and also some source reaction.

## A.2 Reactions and Species Present

In order to properly understand what is happening during EARE or ES deposition, one must not only consider general aspects (above) but, in addition, specifics relating to Ti and $N_2$. Though no plasma discharge is present for the ES method, the discussion below applies to some degree for that case, but radical concentrations will be necessarily lower. The species present at the substrate surface and in the reaction zone must be known to make any attempt at understanding the process of reactive deposition. This varys greatly from one materials system to the next; *e.g.*, the species prenent in an $N_2$ plasma are very different from those in an $O_2$ plasma. Factors such as ionization energy, dissociation energy, electron affinity, and system geometry must be considered, as well as the general notions of volume *vs.* surface reactions discussed above.

### A.2.1 Plasma Discharge Volume

Initially, it is useful to catalogue all possible reactions between the *primary* reactants, *i.e.* those purposely introduced. Impurities and their effects will be considered later. The primary reactants in the present case consist of: $N_2$ gas, Ti vapor, and $e^-$. The primary reactions to be concerned with are those of Ti and N with electrons. A list of such reactions is shown in Table A.1 [6] [20] [21] [33]. (Recall that $A^*$ represents an rotational, vibrational, or electronic excite state of A.)

It is useful to remember that in a plasma discharge, the principle of detailed balancing, *viz.*, at equilibrium the forward and reverse rates for all possible reactions are balanced, does not apply [33]. Often a single collision process may dominate over all others such that its forward and reverse rates are balanced. This is the case for free electrons if their density is high. In that case, an effective electron temperature may be defined, $T_e$, that describes the electron plasma, and its velocity distribution will be approximately Maxwellian. Departures from the Maxwellian ideal occur for two

| Reaction | | ΔE (eV) |
|---|---|---|
| Ionization | $N_2 + e^- \rightleftharpoons N_2^+ + 2e^-$ | 15.6 |
| | $N + e^- \rightleftharpoons N^+ + 2e^-$ | 144.6 |
| | $Ti + e^- \rightleftharpoons Ti^+ + 2e^-$ | 683 |
| Dissociation | $N_2 + e^- \rightleftharpoons 2N + e^-$ | 9.82 |
| $e^-$ Attachment | $N + e^- \rightleftharpoons N^-$ | 0.546 |
| | $Ti + e^- \rightleftharpoons Ti^-$ | 0.196 |
| Electronic Excitation | $A + e^- \rightleftharpoons A^* + e^-$ | – |

Table A.1: Plasma Volume and Surface Reactions: $N_2$, Ti, and $e^-$. (Compiled from [6] [20] [21] [33]. $A^*$ represents an excited state.)

primary reasons: the electric field, which transfers some electrons to higher energies; and inelastic collisions, which transfer some electron to lower energies. The latter is of the most practical importance, and it leads to an effect known as collisional tail depopulation. The depopulation of high energy electrons due to inelastic collisions can be quite severe, effectively limiting the electron plasma to low energies. For example, cross section data for $N_2$ indicate a peak in the vibrational cross section at 2eV which is almost impenetrable. Unless very high fields and relatively low pressures are used, the electron energy in an $N_2$ plasma is effectively limited to <2eV.

In the case of other species (*i.e.*, Ti and $N_2$), several factors will determine what reactions will dominate, and in what region(s). Based on energy of formation for the species listed, it is clear that some reactions will be relatively minor, such as the formation of $N^+$. Not only is a relatively large amount of energy required, in excess of 100 eV, but the excess of $e^-$ in the chamber would quickly neutralize any $N^+$ which was created. Similarly, the ionization of $N_2^+$ is rather unlikely. This again relates to the $N_2$ collision cross section. Since ionization energies are much greater than dissociation, a nitrogen plasma have a much higher degree of dissociation - as high as 70% [33] - than ionization (typically >0.01%). A further subtlety arises when one considers that atomic species cannot recombine in two-body gas phase collisions. This is because a single species formed cannot conserve both energy and momentum [33]. Thus, dissociation will dominate in the $N_2$ plasma, and, further, the atomic nitro-

gen or nitrogen radicals formed will have an extremely long lifetime (as they cannot recombine). Atomic radicals may only recombine at surfaces, such as the substrate or chamber walls. Figure A-1 schematically shows $N_2$ plasma reactions [1]. From table A.1 and fig. A-1, it can be readily seen that the dominant species in a nitrogen plasma will be $N^-$, N, and, to a lesser extent $N_2^+$. Augmenting this is the fact that electronically excited states in molecules will tend to weaken bonding that can result in dissociation [33].

Once the predominant species are determined, they must be examined for further reactions. For example, rate constants for ion-ion reactions of positive and negative ions will be fast due to Coulomb forces. Thus, any $N_2^+$ formed will rapidly undergo dissociative recombination ($N_2^+ + e^- \rightleftharpoons 2N$). Ion-electron reactions such as this ususally occur predominantly at surfaces [33]. Electron densities are sufficiently low that electron-ion volume recombination, and impact ionization *via* excited states may be ignored. Thus, considering all factors, the predominant reactions will be electron impact ionization, and some degree of dissociation, with ionized and radical species reacting and recombining at the surfaces (*i.e.* chamber walls, substrate).

In addition to the nitrogen plasma, it is important to remember that there also exists a Ti vapor flux within the reaction volume, though at a much lower partial pressure. However, ionization and exication of the Ti will still occur, and a distinct Ti plasma may sometimes be oberved for higher deposition rates (*i.e.*, higher Ti partial pressure). Similar to the case for $N_2$, Ti vapor will prefer to form $Ti^-$ radicals (see table A.1), as the threshold energy for $Ti^+$ formation is rather large. Excited states may also be formed for Ti atoms or radicals (*e.g.* Ti*). As with ion-electron recombination, molecular recombination occurs at the surfaces. Potentially, molecular recombination may occur in the reaction volume, but this is not relevant in the present case. Recall, also, that since Ti and atomic N are forbidden to recombine,

[1]Note that combinations of the above reactions are possible, but may not involve recombination of atomic species.

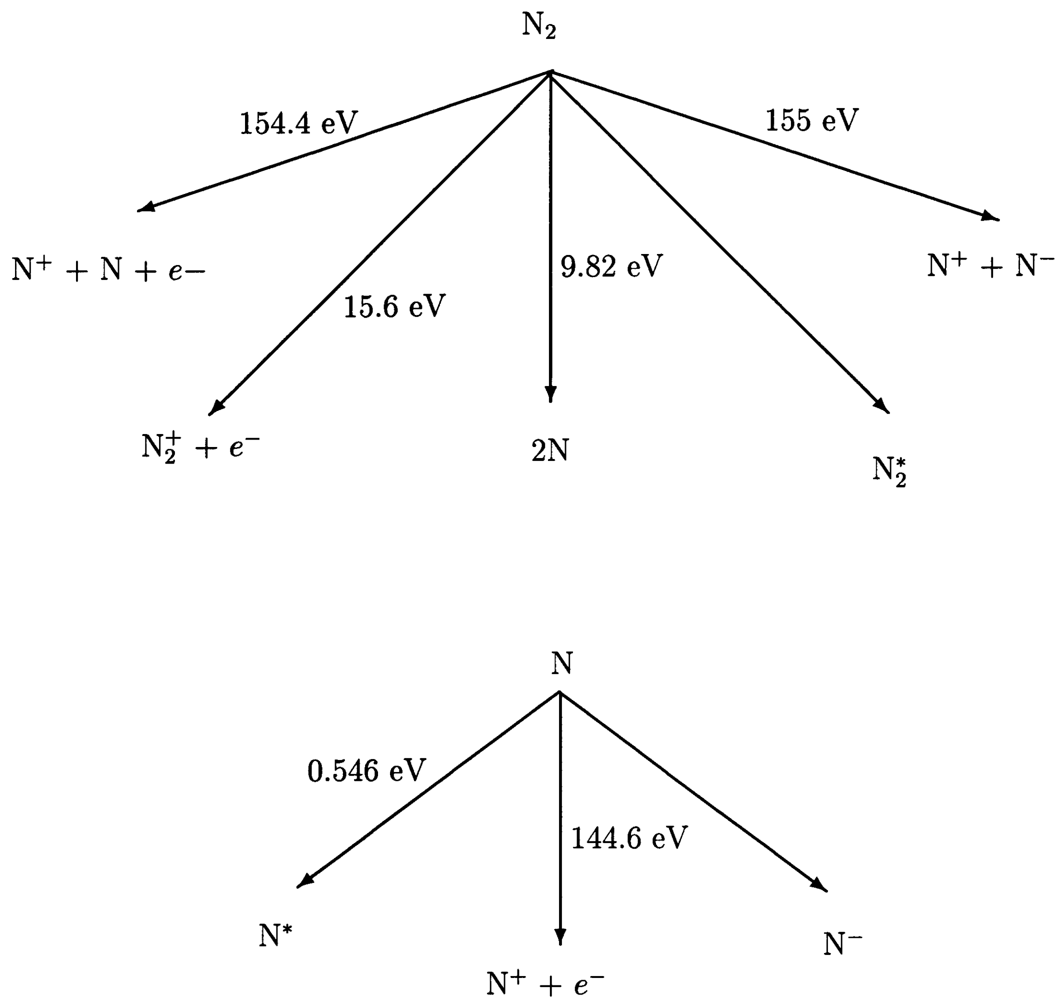


Figure A-1: Schematic of $N_2$ Plasma Reactions.

TiN formation must occur only at surfaces.

### A.2.2 Plasma-Surface Interactions

For this work, the plasma surface interactions are uniquely important. Since the substrate is positively biased in this case, it will be subject to electron and negative ion bombardment ($N^-$ and $Ti^-$) in addition to bombardment by neutrals ($N_2$, Ti). The energies these species bring to the surface is ~10 eV or more, which is significantly higher than, *e.g.*, surface binding energy, defect formation, or sputtering threshold energies. This leads to a whole host of possible substrate and film modifications. Low energy ion and neutral bombardment can lead to sputter desorption of adsorbed impurities from the substrate or film, primarily because such adsorbed species have low threshold energies and high sputter yields compared to the substrate. Higher energy ions or neutrals can penetrate the substrate or film and become trapped, while high energy ions (~few hundred eV) can modify the coating microstructure. Bombardment by energetic particles can generate preferential absorption sites, and increase adatom mobility *via* adding energy to the surface. Energetic bombardment can also cause surface dissociation, thereby stimulating reactions with either the substrate or reactant species. For reactive deposition, this ion and electron stimulated surface chemistry is of vital importance [33]. Essentially, nearly any film property will be modified in some manner as a result of plasma-surface interactions [6].

Critical in the present case are two processes: interaction of the substrate with $N_2$ plasma, and Ti-N surface reactions. In the first case, it is during the pre-deposition "activation" phase that the $SiO_2$ or Si substrate forms a surface layer of $Si_3N_4$ [7]. Energetic electron and N ion bombardment increases the reactivity of the Si or $SiO_2$ surface, and stimulates the formation of a nitride layer. In the case of Si, this is simply plasma nitriding of the surface layer. In the case of $SiO_2$, however, the nitride formation from $SiO_2$ is an unfavorable reaction (see table 2.3). The formation of the nitride is possible only by electronic activation of the surface. It is this nitride forma-

tion which is viewed as responsible for the extraordinary adhesion of TiN to glass for ES samples [7], whereas TiN films by other methods typically have poor adhesion.

As for second case, Ti-N surface reactions, the situation is slightly less clear. No TiN can form within the volume (see above), therefore the surface reactions are of key importance. Ti or $Ti^-$ arriving on the surface, possibly already electronically excited, may be ionized or excited once on the surface due to electron and ion bombardment. Once on the surface, $Ti^-$ will be deionized to Ti (and likewise for $N^-$) since the substrate is positively biased. With the bombardment of $N^-$ and other nitrogen species, the reaction between Ti and N should proceed rather rapidly since both states are excited. In addition, surface mobility of all species should be quite high; thus, both the thermodynamics and kinetics of TiN formation become extremely favorable.

# Appendix B

# X-ray Diffraction Data

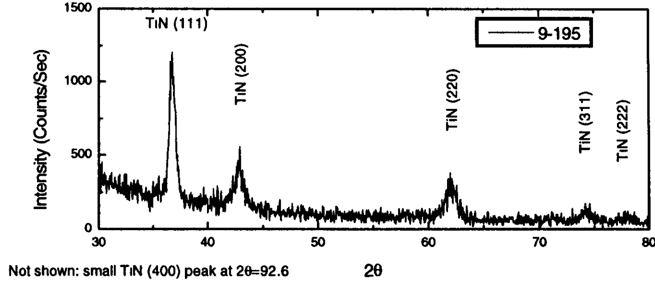

9-195
TiN (111)
TiN (200)
TiN (220)
TiN (311)
TiN (222)
Intensity (Counts/Sec)
2θ
Not shown: small TiN (400) peak at 2θ=92.6


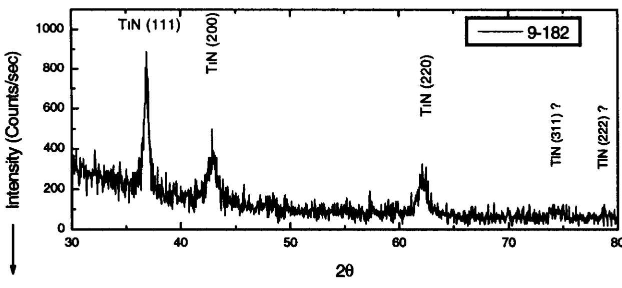

9-182
TiN (111)
TiN (200)
TiN (220)
TiN (311) ?
TiN (222) ?
Intensity (Counts/sec)
2θ


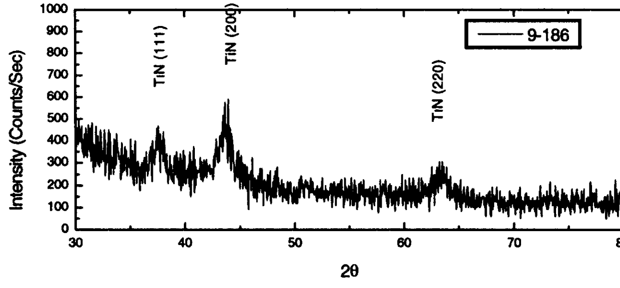

9-186
TiN (111)
TiN (200)
TiN (220)
Intensity (Counts/Sec)
2θ


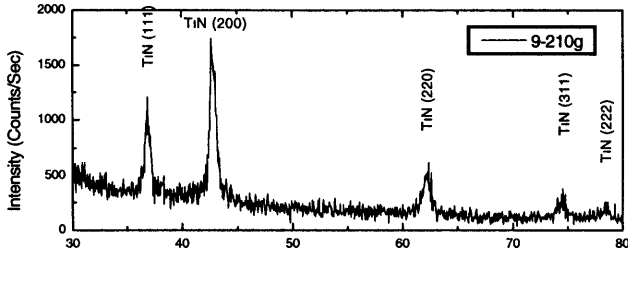

9-210g
TiN (111)
TiN (200)
TiN (220)
TiN (311)
TiN (222)
Intensity (Counts/Sec)


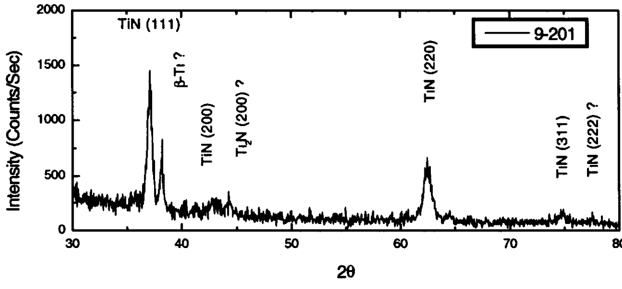

9-201
TiN (111)
β-Ti ?
TiN (200)
Ti2N (200) ?
TiN (220)
TiN (311)
TiN (222) ?
Intensity (Counts/Sec)
2θ


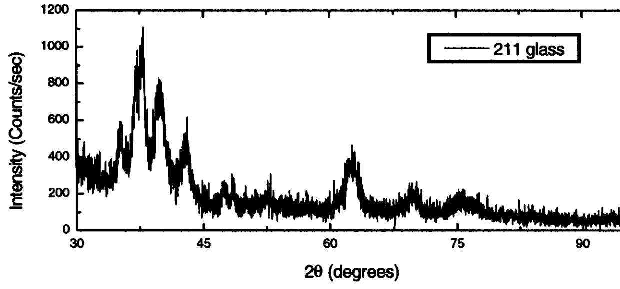

211 glass
Intensity (Counts/sec)
2θ (degrees)


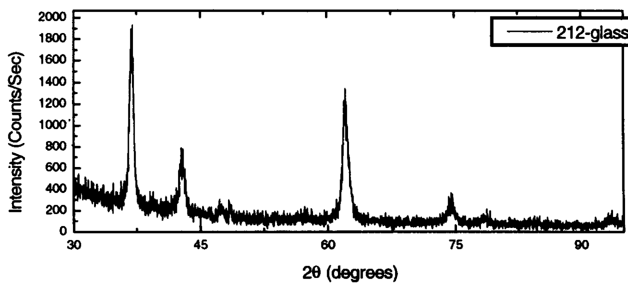

212-glass
Intensity (Counts/Sec)
2θ (degrees)


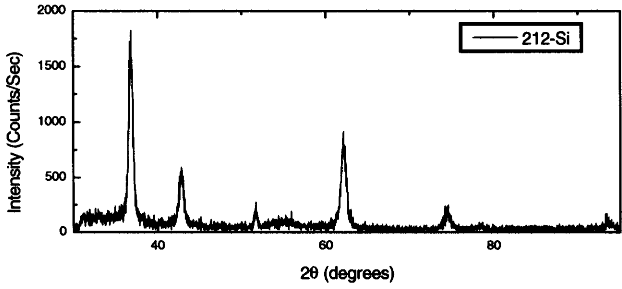

212-Si
Intensity (Counts/Sec)
2θ (degrees)


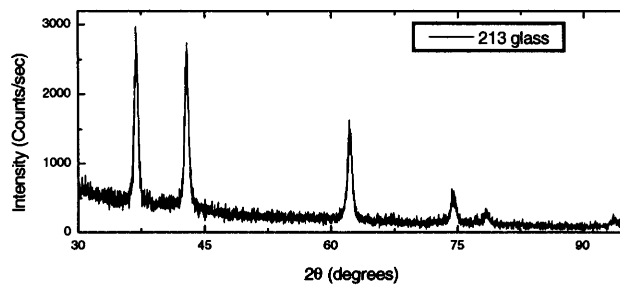

213 glass
Intensity (Counts/sec)
2θ (degrees)


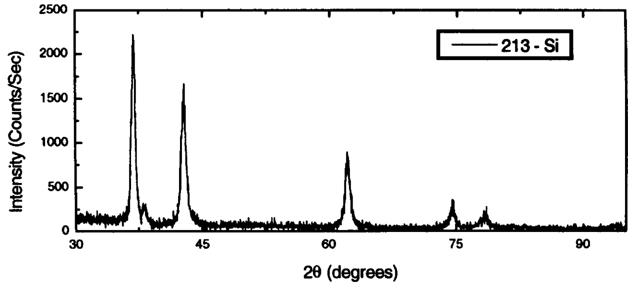

213 - Si
Intensity (Counts/Sec)
2θ (degrees)


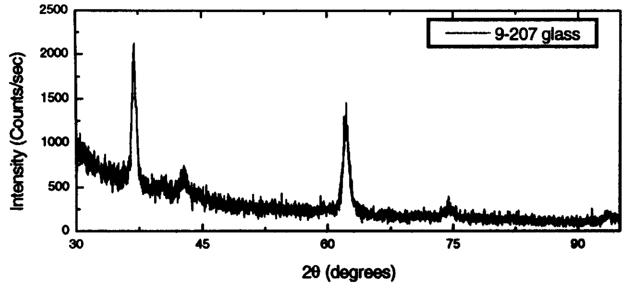

9-207 glass
Intensity (Counts/sec)
2θ (degrees)


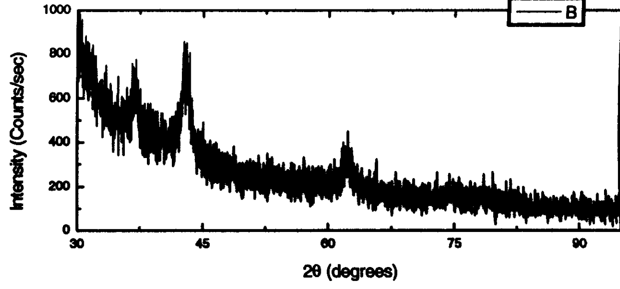

B
Intensity (Counts/sec)
2θ (degrees)


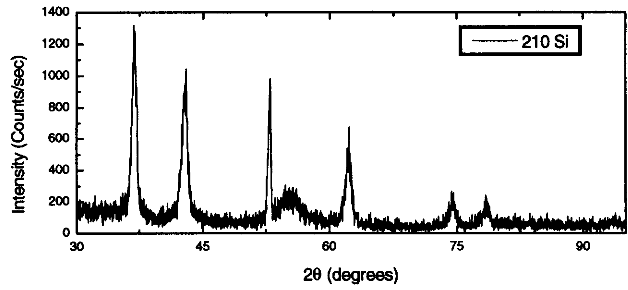

210 Si
Intensity (Counts/sec)
2θ (degrees)

# Appendix C

# Resistivity vs. Temperature Data

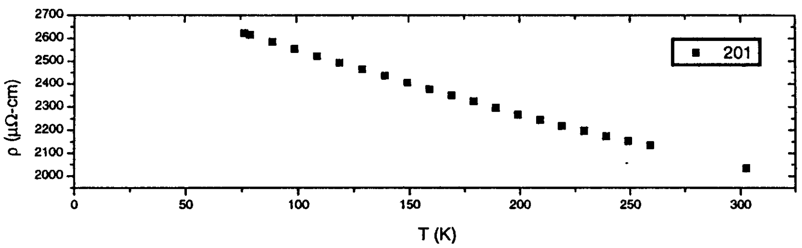

ρ (μΩ-cm)
T (K)
201


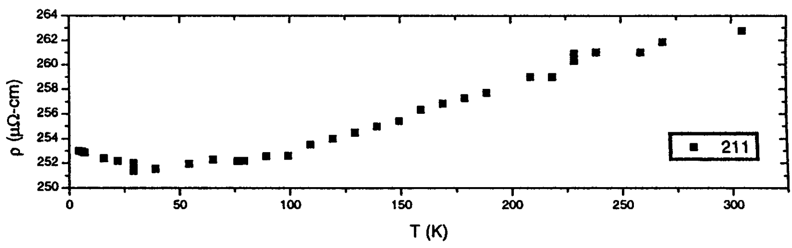

ρ (μΩ-cm)
T (K)
211


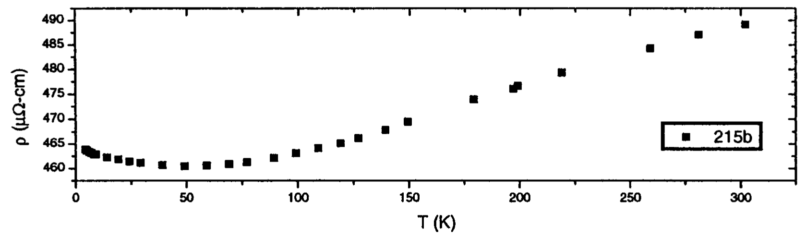

ρ (μΩ-cm)
T (K)
215b


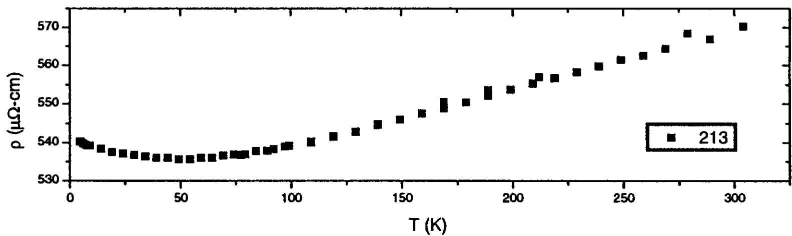

ρ (μΩ-cm)
T (K)
213


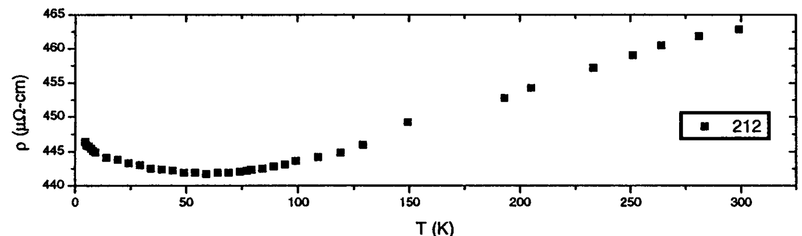

ρ (μΩ-cm)
T (K)
212


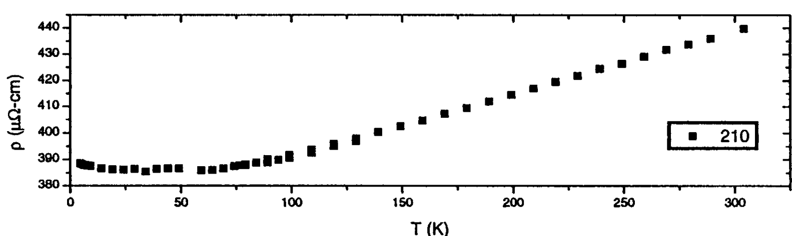

ρ (μΩ-cm)
T (K)
210


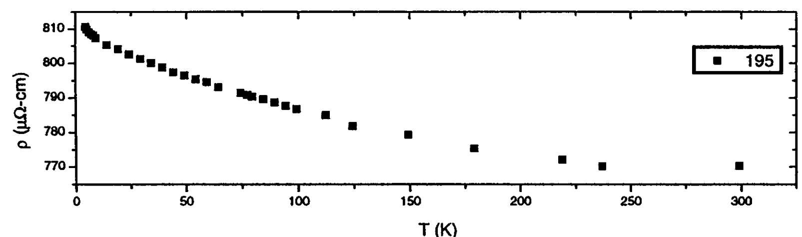

ρ (μΩ-cm)
T (K)
195


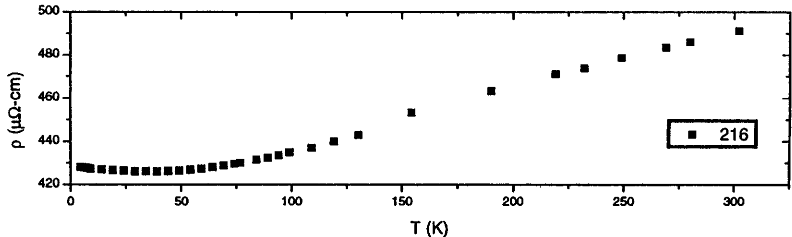

ρ (μΩ-cm)
T (K)
216


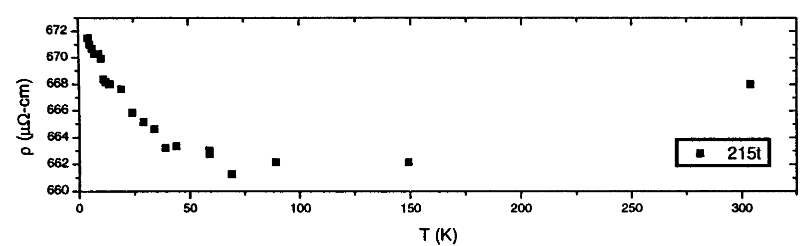

ρ (μΩ-cm)
T (K)
215t